Atmospheric
Chemistry
and Physics
Discussions

Open Access

EGU

Design and evaluation of CO_2 observation network to optimize surface CO_2 fluxes in Asia using observation system simulation experiments

Jun Park[1] and Hyun Mee Kim[1]

[1]Atmospheric Predictability and Data Assimilation Laboratory, Department of Atmospheric Sciences, Yonsei University, Seoul, Republic of Korea

Correspondence to: Hyun Mee Kim (khm@yonsei.ac.kr)

Abstract. Continuous efforts have been made to monitor atmospheric CO_2 as it is one of the most influential greenhouse gases in Earth's atmosphere. Inverse modeling, which is one of the methods to carry out such monitoring, derives estimated CO_2 mole fractions in the air from calculated surface carbon fluxes using model and observed CO_2 mole fraction data. Although observation data is crucial for successful modeling, comparatively fewer in-situ observation sites are located in Asia compared to Europe or North America. Based on the importance of the terrestrial ecosystem of Asia for global carbon exchanges, more observation stations and an effective observation network design are required. In this paper, several observation network experiments were conducted to optimize the surface carbon flux of Asia using CarbonTracker and observation system simulation experiments (OSSE). The impacts of the redistribution of and additions to the existing observation network of Asia were evaluated using hypothetical in-situ observation sites. In the case of the addition experiments, 10 observation stations, which is a practical number for real implementation, were added through three strategies: random addition, the influence matrix (i.e., self-sensitivity), and ecoregion information within the model. The simulated surface carbon flux in Asia in summer can be improved by redistributing the existing observation network. The addition experiments revealed that considering both the distribution of normalized self-sensitivity and ecoregion information can yield better simulated surface carbon fluxes compared to random addition, regardless of the season. This study provides a diagnosis of the existing observation network and useful information for future observation network design in Asia to estimate the surface carbon flux, and also suggests the use of an influence matrix for designing carbon observation networks. Unlike other previous

observation network studies with many numerical experiments for optimization, comparatively fewer experiments were required in this study. Thus, the methodology used in this study may be used for designing observation networks for monitoring greenhouse gases at both continental and global scales.

1. Introduction

5   CO_2 is one of the most influential greenhouse gases in Earth's atmosphere (Lacis et al., 2010). Thus, monitoring CO_2 is very important to understand and constrain CO_2 in the atmosphere. To monitor atmospheric CO_2 precisely, continuous efforts are necessary. Inverse modeling, one of the methods to complete this mission, uses observation data and transport models to estimate the sources and sinks of surface carbon flux and associated atmospheric CO_2 mole fractions (Enting, 2002; Gurney et al., 2002).

10 Bayesian synthesis (Enting, 2002), four dimensional variational data assimilation methods (4DVar; Chevallier et al., 2009a, 2009b, 2010; Kou et al., 2017), and Ensemble Kalman Filter (EnKF; Peters et al., 2005, 2007, 2010; Feng et al., 2009, 2016; Kang et al., 2011, 2012; Peylin et al., 2013; Kim et al., 2014a, 2014b, 2017, 2018a, 2018b) have been implemented and utilized to conduct inverse modeling. By comparing 13 inverse modeling systems, Peylin et al. (2013) showed that simulation results were similar

15 to each other for regions with many observations, but dissimilar for regions with sparse observation coverage (e.g. the tropics and southern hemisphere).

    The terrestrial system in the northern hemisphere is crucial for global carbon exchanges, and Asia covers the largest area in the northern hemisphere (Hayes et al., 2011; Le Quéré et al., 2018). Asia also includes the Siberian region, which represents one of the significant areas for sources and sinks of

20 atmospheric CO_2 (Schulze et al., 1999; Houghton et al., 2007; Tamocai et al., 2009; Kurganova et al., 2010; Schepaschenko et al., 2011, Siewert et al., 2015). Thus, the precise estimation of the surface carbon flux in Asia is highly necessary and required to fully understand global carbon exchanges. However, comparatively fewer in-situ observation sites are located in Asia compared to Europe and North America. Although the Center for Global Environmental Research (CGER) of the National Institute for

25 Environmental Studies (NIES) in Japan, collaborating with the Russian Academy of Science (RAS), has built nine tower observation sites (Japan-Russia Siberian Tall Tower Inland Observation Network, JR-STATION) in Asia, and several studies have been conducted using continuously observed atmospheric

CO_2 and CH_4 mole fractions since 2002 (Saeki et al., 2013; Sasakawa et al., 2010, 2013; Kim et al., 2017), the towers of the JR-STATION are mainly located in the Siberian region. In addition, eight stations of the JR-STATION are located in western Siberian. These JR-STATION sites, therefore, do not seem to be well-suited for optimizing the surface carbon flux for the entire Asia region, and in-situ observation sites in Asia are still fewer compared to those in Europe or North America, even when the JR STATION sites are considered.

In the meantime, the satellite-retrieved dry-air column-average mole fraction of CO_2 (XCO_2) could be used to supplement observations in the sparse observation regions, including Asia (Chevallier et al., 2009a, 2009b, 2010; Maksyutov et al., 2013; Reuter et al., 2014; Feng et al., 2016). However, by comparing CO_2 mole fractions observed in four World Meteorological Organization (WMO) Global Atmosphere Watch (GAW) stations in China to satellite-retrieved products from the Greenhouse Gases Observing Satellite (GOSAT), Cheng et al. (2018) reported that satellite-retrieved CO_2 mole fractions showed similar seasonal variations to those of in-situ observations but the magnitudes retrieved from the satellite were comparatively lower than those of in-situ observations. Assimilating XCO_2 data is therefore generally less effective than assimilating in-situ observations (Chevallier et al., 2009a; Fischer et al., 2017). In contrast, Maksyutov et al. (2013) noted that uncertainties in surface CO_2 flux estimations in sparse in-situ observation regions could be reduced when in-situ observations and GOSAT observation data were used simultaneously. In particular, Fischer et al. (2017) showed that uncertainties in surface CO_2 flux estimation could be further decreased, even for the regions with in-situ observation sites, when in-situ observations and satellite-retrieved observations are used together. Thus, in-situ observation networks need to be well established to better utilize non in-situ observations like XCO_2.

Observation system simulation experiments (OSSE), using simulated observation data, provide an opportunity to evaluate the impact of observation data from the current and potential observation sites on the performance of the modeling system (Yang et al., 2014; Byrne et al., 2017; Wang et al., 2018; Wu et al., 2018). Thus, OSSE can be used to evaluate the performance of current observation networks and to design future observation networks. Although several studies have been conducted to achieve this aim, most observation network design studies were restricted to comparatively smaller national scales such as Australia, California in the USA, and South Africa (Ziehn et al. 2014, 2016; Lucas et al., 2015; Nickless

et al., 2015). As potential observation sites are few in these studies due to the relatively small study area, these studies suggest an optimized network derived from a myriad of calculations using the incremental optimization (IO) and the genetic algorithm (GA). Due to time and computing restraints, the IO and GA methods seem ineffective or unfeasible for designing the observation network on continental scales like

5   Asia.

The influence matrix (i.e., analysis sensitivity or self-sensitivity) denotes the sensitivity of the analysis to the observations (Cardinali et al., 2004; Liu et al., 2009; Kim et al. 2014a; Kim et al. 2017). Similar to the numerical weather prediction (NWP), the relative impact of each CO_2 observation for the optimized surface carbon flux can be calculated (Kim et al., 2014a, 2017) and used as a strategy for selecting

10   potential sites of CO_2 mole fraction observations. Although Wang et al. (2018) showed the potential impact of adding observation sites on the existing [14]CO_2 sites in Europe using OSSE, they considered a considerable number of observation sites, which does not seem to be feasible in the near future. Moreover, studies on diagnosing the current CO_2 mole fraction observation network and evaluating the impact of adding and redistributing in-situ CO_2 mole fraction observation sites in Asia are few up to this time.

15   Considering the importance of the Asia region for global carbon exchange, studies on the observation network design in Asia to accurately estimate the surface carbon flux are highly necessary. Such observation network studies could also provide helpful information for researchers and administrators who design the future observation network under practical conditions.

In this study, OSSE were conducted using CarbonTracker (CT) to identify a better in-situ observation

20   network for the purpose of optimizing surface carbon flux estimation in Asia. Based on the hypothetical simulated observations, redistribution and addition experiments were performed to evaluate the performance of the existing observation network and the impact of additional observation sites, respectively. In the case of addition experiments, random addition and addition based on influence matrix (self-sensitivity) as well as ecoregion information of the model were considered as strategies. Section 2

25   briefly introduces the CT, influence matrix, hypothetical observations, experimental framework, and verification methods. Section 3 presents the results of the observation network design experiments, and Sect. 4 provides a summary and the conclusions of this study.

2. Methodology

2.1 CarbonTracker and data assimilation methods

CT2013B, developed by the Earth System Research Laboratory (ESRL) at the National Oceanic and Atmospheric Administration (NOAA), was used for this study. CT2013B estimates the surface carbon flux using inverse modeling and has been widely used to calculate surface carbon fluxes in North America, Europe, and Asia (Peters et al., 2004, 2005, 2007, 2010; Kim et al., 2012, 2014a, 2014b, 2017; Cheng et al., 2013; Kim et al., 2016, 2018a, 2018b).

CT2013B consists of a priori flux modules, a transport model (TM5), observation data, and EnKF data assimilation. The estimated surface CO_2 fluxes are mainly calculated from flux modules composed of biosphere, ocean, fossil fuel, and fire fluxes. The optimized grid-point surface CO_2 fluxes within TM5 were derived as follows:

$$F(x, y, t) = \lambda_r \cdot F_{\text{bio}}(x, y, t) + \lambda_r \cdot F_{\text{ocean}}(x, y, t) + F_{\text{ff}}(x, y, t) + F_{\text{fire}}(x, y, t) \qquad (1)$$

where $F_{\text{bio}}(x, y, t)$, $F_{\text{ocean}}(x, y, t)$, $F_{\text{ff}}(x, y, t)$, and $F_{\text{fire}}(x, y, t)$ denote a priori emissions of the biosphere, ocean, fossil fuel, and fires, respectively; λ_r is the scaling factor with a 1-week resolution for ecoregions; x, y, and t denote the zonal direction, the meridional direction, and time, respectively. λ_r is used for optimization of the surface CO_2 flux through interactions with a priori emissions of the biosphere and the ocean. Thus, EnKF data assimilation in CT2013B optimizes not surface CO_2 fluxes but the scaling factor. This means that the optimization of the scaling factors that were assigned to the 240 ecoregions of the earth is crucial for the estimation of simulated surface CO_2 fluxes. The ecoregions are defined as the mix of the modified 19 vegetation types from Olson et al. (1992) and 11 Transcom regions (Gurney et al., 2002) on land, with 30 ocean regions. As all 19 vegetation types are not used for the 11 Transcom regions, the number of effective ecoregions is 156 (Peters et al., 2010).

TM5 is an off-line transport model used to calculate the transport of CO_2 (Krol et al., 2005), which utilizes the atmospheric fields of the ERA-interim reanalysis data of the European Centre for Medium-Range Weather Forecasts (ECMWF). TM5 utilizes the estimated surface CO_2 fluxes at each grid-point suggested in Eq. (1) to calculate the spatiotemporal distribution of the atmospheric CO_2. In addition, it

also calculates the model counterparts corresponding to the same location and time of observation data, which are used for the data assimilation process. A two-way nested grid was used in this study to optimize surface CO_2 fluxes in Asia (Fig. 1). Table 1 summarizes the priori flux emissions used for the flux module and describes the TM5 setup.

5　　An Ensemble Square Root Kalman Filter (EnSRF), one of the EnKF data assimilation methods (Evensen, 1994; Whitaker and Hamill, 2002), was employed in this study to optimize the scaling factor. EnSRF assimilates observation data one by one, and updates the analysis of ensemble mean and perturbations separately based on the following equations as:

10
$$\overline{x}_t^{\,a} = \overline{x}_t^{\,b} + \mathbf{K}(y^o - \mathbf{H}(\overline{x}_t^{\,b})), \tag{2}$$

$$x'_i^{\,a} = x'_i^{\,b} - \tilde{\mathbf{k}}\mathbf{H}(x'_i^{\,b}), \tag{3}$$

where x^a and x^b describe the analysis and background value of the state vector (x); $\overline{x}$ and x' are the ensemble mean and perturbation of the state vector; y^o is the observation vector; and $\mathbf{H}$ describes the
15　observation operator that transforms the state vector from the model space to the observation space. TM5 acts as the observation operator in CT2013B (Krol et al., 2005; Peters et al., 2005; Kim et al., 2016, 2018a). $\mathbf{K}$ and $\tilde{\mathbf{k}}$ denote the Kalman gain matrix and the reduced Kalman gain calculated as:

$$\mathbf{K} = (\mathbf{P}_t^{\,b}\mathbf{H}^T)(\mathbf{H}\mathbf{P}^b\mathbf{H}^T + \mathbf{R})^{-1}, \tag{4}$$

20　$$\tilde{\mathbf{k}} = \mathbf{K} \cdot \alpha, \tag{5}$$

where $\mathbf{P}_t^{\,b}$ is the background error covariance; $\mathbf{R}$ is the observation error covariance for each observation; and α is a scalar value that is multiplied to Kalman gain matrix at every calculation of the analysis, defined as:

25

$$\alpha = (1 + \sqrt{\frac{\mathbf{R}}{\mathbf{H}\mathbf{P}_t^{\,b}\mathbf{H}^T + \mathbf{R}}})^{-1}. \tag{6}$$

By calculating the ensemble mean and perturbation independently, the underestimation of the analysis error covariance could be prevented (Whitaker and Hamill, 2002; Kim et al., 2012). $\mathbf{P}_t^{\,b}\mathbf{H}^T$ and $\mathbf{HP}_t^{\,b}\mathbf{H}^T$ can be calculated as:

5

$$\mathbf{PH}^T \approx \frac{1}{m-1}(\boldsymbol{x'}_1, \boldsymbol{x'}_2, \cdots, \boldsymbol{x'}_m) \cdot (\mathbf{H}\boldsymbol{x'}_1, \mathbf{H}\boldsymbol{x'}_2, \cdots, \mathbf{H}\boldsymbol{x'}_m)^T, \tag{7}$$

$$\mathbf{HP}^b\mathbf{H}^T \approx \frac{1}{m-1}(\mathbf{H}\boldsymbol{x'}_1, \mathbf{H}\boldsymbol{x'}_2, \cdots, \mathbf{H}\boldsymbol{x'}_m) \cdot (\mathbf{H}\boldsymbol{x'}_1, \mathbf{H}\boldsymbol{x'}_2, \cdots, \mathbf{H}\boldsymbol{x'}_m)^T, \tag{8}$$

where m is the number of ensemble members.

10   Unlike the approach of NWP, the time for CO_2 dispersing around the atmosphere needs to be considered for carbon data assimilation. Accordingly, a time lag is introduced in updating the scaling factor during the data assimilation process to consider the information for analysis time as well as for pre-analysis time. A time lag of five weeks is employed in this study, consistent with previous studies (Peters et al., 2007, 2010, Kim et al., 2012, 2014a, 2014b, 2017).

15   In the EnSRF, the covariance localization method is necessary to reduce the impact of the sampling error due to the limited size of the ensemble and to avoid filter divergence due to the underestimation of the background error covariance (Houtekamer and Mitchell, 2001). The statistical method is applied in this study because calculating the physical distance between scaling factors is not feasible. In this method, a Student's t test is applied on the correlations between the ensemble of the model CO_2 concentrations

20   and the ensemble of the scaling factors, and the Kalman gain matrix is then made to be zero for the cases where it has an insignificant statistical t value (i.e. 95 % significance level), to exclude those insignificant impacts (Peters et al., 2007).

The optimized mean scaling factor after one analysis cycle is used as one of the prior mean scaling factors for the next analysis step as:

25

$$\lambda_t^{\,b} = \left(\frac{\lambda_{t-2}^{\,a} + \lambda_{t-1}^{\,a} + 1}{3}\right), \tag{9}$$

Atmospheric
Chemistry
and Physics
Discussions
Open Access
EGU

where, λ_t^{b} is a prior mean scaling factor for the current analysis step; and λ_{t-2}^{a} and λ_{t-1}^{a} denote posterior mean scaling factors of previous analysis cycles. The information of current analysis propagates to the next step using Eq. (9) (Peters et al., 2007).

2.2 Influence matrix

The influence matrix of the EnKF system can be calculated as described in Liu et al. (2009) and Kim et al. (2014a). The analysis of the state vector and the influence matrix ($\mathbf{S}^{\text{o}}$) that shows the contribution of the observation vector ($\boldsymbol{y}^{\text{o}}$) to the analysis at the observation space ($\boldsymbol{y}^{\text{a}}$) can be defined as:

$$\mathbf{x}^{\text{a}} = \mathbf{K}\boldsymbol{y}^{\text{o}} + (\mathbf{I}_n - \mathbf{KH})\boldsymbol{x}^{\text{b}}, \tag{10}$$

$$\mathbf{S}^{\text{o}} = \frac{\partial \boldsymbol{y}^{\text{a}}}{\partial \boldsymbol{y}^{\text{o}}} = \mathbf{K}^{\text{T}}\mathbf{H}^{\text{T}} = \mathbf{R}^{-1}\mathbf{HP}^{\text{a}}\mathbf{H}^{\text{T}}, \tag{11}$$

where, $\mathbf{I}_n$ is the identity matrix corresponding to the size of observation. The influence matrix is proportional to the analysis error covariance and inversely proportional to the observation error covariance. Using Eq. (8), $\mathbf{S}^{\text{o}}$ is expressed as:

$$\mathbf{S}^{\text{o}} = \mathbf{R}^{-1}\mathbf{HP}^{\text{a}}\mathbf{H}^{\text{T}} = \frac{1}{m-1}\mathbf{R}^{-1}(\mathbf{HX}^{\text{a}})(\mathbf{HX}^{\text{a}})^{\text{T}}, \tag{12}$$

where $\mathbf{HX}^{\text{a}}$ is the analysis of the ensemble perturbation at the observation space. The ith component of $\mathbf{HX}^{\text{a}}$ is defined as:

$$\mathbf{HX}_i^{\text{a}} \cong h(\boldsymbol{x}_i^{\text{a}}) - \frac{1}{m}\sum_{i=1}^{m} h(\boldsymbol{x}_i^{\text{a}}), \tag{13}$$

where $\boldsymbol{x}_i^{\text{a}}$ is the ith member of the analysis ensemble; and $h(\cdot)$ denotes the linearized or non-linearized observation operators. If there are no correlations between observation errors, the diagonal element of this influence matrix (i.e. self-sensitivity) is calculated as:

Atmospheric
Chemistry
and Physics
Discussions

$$\mathbf{S}_{jj}{}^{o} = \frac{\partial \boldsymbol{y}_j{}^{a}}{\partial \boldsymbol{y}_j{}^{o}} = \left(\frac{1}{m-1}\right)\frac{1}{\sigma_j{}^2}\sum_{i=1}^{m}(\mathbf{HX}_i{}^{a})_j \cdot (\mathbf{HX}_i{}^{a})_j, \tag{14}$$

where $\sigma_j{}^2$ is the observation error variance for the jth observation.

According to Liu et al. (2009), $\mathbf{S}^{o}$ has a value between 0 and 1, which shows the contribution of an observation to the analysis. If $\mathbf{S}^{o}$ is close to 0, the analysis is mainly derived from the background. In contrast, the influence of observation data to the analysis increases as $\mathbf{S}^{o}$ goes to 1. The self-sensitivity was used as a criterion for selecting the observation locations in designing the observation network.

2.3 Simulated hypothetical observation and experimental setup

In this paper, simulated hypothetical observations were created and used to design the observation network. Simulated hypothetical observations with similar values and seasonal variations compared to real CO_2 observations were generated by combining two model CO_2 mole fractions from the experiment conducted with real NOAA observation data (EXTASI) and the experiment with a fixed scaling factor of 1 (SF1).

Figure 2 shows the station-averaged time series of CO_2 mole fractions from real observations (OBS), EXTASI, SF1, and an average of EXTASI and SF1 (i.e., simulated hypothetical observations: TRUE, hereafter). The time series of EXTASI is the closest to that of OBS, whereas that of SF1 with a static scaling factor (i.e., 1) differs from OBS, particularly in summer. The time series of TRUE is located between that of EXTASI and SF1, which implies that the difference between TRUE and OBS is smaller compared with that between SF1 and OBS. TRUE is the simulated hypothetical observation that is similar to the EXTASI assimilating real NOAA observation data, but is not the same as the EXTASI. This setup prevents EXTASI from having an advantage in the observation network experiments. If TRUE is the same as EXTASI, then assimilating TRUE data at the observation locations used in EXTASI would render the observation network used in EXTASI the optimal network in terms of several verification measures used in this study.

Each hypothetical observation site has one CO_2 observation per day and exists within the limited Asia domain shown in Fig. 1. On the basis of the nautical time zone, the simulated values around afternoon (13 LST) in the mid-latitudes in the northern hemisphere are averaged and utilized as TRUE data. The observation height of TRUE data at each site is set to 5 meters greater than the model elevation of the grid-point in order to use the observation operator for flask observation developed in NOAA. Moreover, each observation site is more than 1,000 km apart from other sites, located lower than 2,000 meters above sea level, and located on the land regions in the Transcom Region from Gurney et al. (2002). This configuration was made to consider real-world constraints to optimize the surface carbon fluxes in Asia. Model-data-mismatch (MDM) was set to 3, consistent with the previous setting of 3 for continuous observation site types (Peters et al., 2007; Kim et al., 2014b, 2017).

All simulation results were produced under identical conditions except for the observation locations and data. 150 ensemble members were used for data assimilation, and experiments were carried out from 27 September 2007 to 4 January 2009. The first three months of the experiments were considered as the spin-up period, thus the analysis was conducted from 27 December 2007 to 4 January 2009.

As the experimental results depend on the distribution of observation sites, appropriate choices of the observation network are important. Experiments are therefore configured to investigate the impact of redistributing observation sites of CT2013B (hereafter, existing observation sites or network) and that of adding extra observation sites to the existing observation network based on random, self-sensitivity, and ecoregion information. Figure 3 shows the hypothetical observation networks used in this study. Figure 3a presents the distribution of seven observation sites in Asia from the observation network of CT2013B, which are mostly located between 30 °N and 45 °N. The experiment and simulation results using this observation network were denoted as CNTL. Since the CNTL could have disadvantages due to the use of real observation information (i.e. the observation height of simulated sites are always above 5 meters from model topography, but this is not the case for CNTL), an additional experiment identical to CNTL, except that the observation heights were assigned above 5 meters from the model topography in the same way as for hypothetical observations, was also conducted and denoted as CNTL_MOD. Figures 3b, c, and d show the distribution of three observation networks, in which the seven observation sites in Asia are

Atmospheric
Chemistry
and Physics
Discussions

randomly redistributed. The average of three random redistribution experiments was denoted as REDIST, to check the impact of the reallocation of the existing observation network.

Figures 3e-m suggest the distributions of the observation networks to examine the impact of adding additional observation sites to the existing observation network. The 10 extra observation sites were added

5 as this number seems realistically viable for the future, considering the cost of operating and maintaining CO_2 observation sites. Specifically, Figures 3e-h show the distribution of three observation networks with additional 10 observation sites added randomly to the existing observation network. The average of these three experiments was denoted as ADD. The experiment adding 10 observation sites to the existing observation network based on self-sensitivity is denoted as the SS experiment (Fig. 3h). The experiment

10 adding 10 observation sites to the existing observation network based on both self-sensitivity and ecoregion information is denoted as the ECOSS experiment (Fig. 3i). The ECOSS experiment was conducted as the scaling factor in CT2013B is updated based on ecoregion, thus only considering self-sensitivity makes the added observation sites cluster in a specific ecoregion and causes disadvantages in optimizing the scaling factor. As the self-sensitivity is generally inversely proportional to the number of

15 assimilated observations (Kim et al., 2014a; 2017), the self-sensitivity normalized by the number of assimilated observations is also considered and utilized. Figures 3j-l show the distributions of the observation network for three experiments that used the normalized self-sensitivity as the selection criterion for added observation sites. The NSS experiment (Fig. 3j) used only the normalized self-sensitivity as the selection strategy. The observation sites of the NECOSS1 (Fig. 3k) and NECOSS2 (Fig.

20 3l) experiments were added based on the normalized self-sensitivity and ecoregion information. The NECOSS1 experiment allocated one or two observation sites per ecoregion, whereas NECOSS2 allocated one observation site per ecoregion. In addition, the observation networks that have observation sites at every 2° intervals on the land (Fig. 3m, ALL experiment) are suggested as the reference to examine the maximum possible impact of additional observation sites.

25 The normalized self-sensitivity is defined as:

$$\mathbf{NS}_{jj}{}^{\mathrm{o}} = \frac{N_j}{N_{\mathrm{ALL}}} \times \mathbf{S}_{jj}{}^{\mathrm{o}}, \tag{15}$$

where N_{ALL} denotes the total count of observation sites of the ALL experiment; and N_j is the number of observation sites that have the same ecoregion as the jth observation site in the ALL experiment. Thus, normalized self-sensitivities were calculated by multiplying self-sensitivities by the ratio of the number of observation sites in a specific ecoregion to that in the ALL experiment.

5   The effect of the redistribution of the existing observation network and adding additional observation sites on the existing observation network can be diagnosed through the experiments detailed above. The method of adding observation sites in the experiments using self-sensitivity and ecoregion information is described in more detail in Sect. 3. Table 2 describes the list of observation network experiments and their relevant information.

10

2.4. Verification method

     The nested model domain over Asia and the verification area (-9.5 °S – 66.5 °N, 60.5 °E – 149.5 °E) are shown in Fig. 1. The optimized surface CO_2 flux in each experiment was verified against the hypothetical surface CO_2 fluxes corresponding to TRUE. Weekly surface CO_2 fluxes were analyzed to 15   evaluate the performance of observation network experiments because the scaling factor has a weekly resolution. The Pearson product-moment correlation coefficient (Pattern Correlation; PC), the bias (BIAS), and the root mean square difference (RMSD) were compared and calculated as:

$$PC = \frac{\sum_{i=1}^{n}(EXP_i - \overline{EXP})(TRUE - \overline{TRUE})}{[(\sum_{i=1}^{n}(EXP_i - \overline{EXP})(\sum_{i=1}^{n}(TRUE_i - \overline{TRUE})))]} , \tag{16}$$

$$20 \quad BIAS = \frac{1}{n}\sum_{i=1}^{n}(EXP_i - TRUE_i), \tag{17}$$

$$RMSD = \sqrt{\frac{1}{n}\sum_{i=1}^{n}(EXP_i - TRUE_i)^2}, \tag{18}$$

where EXP_i and $TRUE_i$ are the surface CO_2 fluxes at the ith model grid-point of an experiment and TRUE, respectively.

To investigate the reduction of uncertainties for each experiment after data assimilation, uncertainty reduction (UR; Peters et al., 2005; Meirink et al., 2008; Chevallier et al., 2009b, Feng et al., 2009; Kim et al., 2014a, 2017, Kim et al., 2018b) was calculated as:

$$UR = \left(1 - \frac{\sigma_{EXP}}{\sigma_{CNTL}}\right) \times 100, \tag{19}$$

where σ_{CNTL} and σ_{EXP} denote 1σ standard deviations of the optimized scaling factor for the CNTL and an experiment. The UR was used to check the improvement of observation network experiments by comparing the posterior uncertainties of experiments with those of CNTL (i.e., the reference experiment).

3. Results

3.1. Effect of an observation network with observation sites redistributed randomly

Figure 4 shows the time series of the three-week moving average of PC, BIAS, and RMSD for surface CO_2 fluxes from the CNTL, CNTL_MOD, and REDIST experiments. Overall, REDIST is closer to TRUE compared to CNTL and CNTL_MOD. The PC of CNTL with the NOAA observation network decreases in mid-April and mid-July, as well as in late August compared to other months. In particular, the PC of CNTL fell to 0.919 in late August (Fig. 4a). This implies that, occasionally, the CNTL experiment may not be effective in optimizing surface CO_2 fluxes in Asia. The PC of CNTL_MOD is quite similar to that of CNTL, except for the much lesser drop in late July compared to CNTL. In contrast, REDIST maintains a higher PC at almost every time compared to CNTL and CNTL_MOD. Particularly in late August, the PC of REDIST is comparatively higher (i.e., 0.955) than those of CNTL and CNTL_MOD (approximately 0.93). This implies that surface CO_2 fluxes in Asia could be optimized more effectively when using the observation sites of the REDIST experiment.

Regarding the BIAS, the three experiments have common variations that increase and decrease around zero, and have high amplitudes in summer compared to other seasons (Fig. 4b). In particular, CNTL_MOD (CNTL) shows the maximum positive BIAS of 23.74 (16.43) in early June. In contrast, the BIAS of REDIST is approximately 10.28 at the same time and maintains its value closest to zero among

Atmospheric
Chemistry
and Physics
Discussions

Open Access

EGU

the three experiments. Considering the impact of BIAS on steady simulations of the model, the time series of BIAS also supports that the observation network of REDIST can perform more reliably in optimizing surface CO_2 fluxes in Asia compared to that of CNTL.

The RMSDs of all three experiments increase much in summer (Fig. 4c). The time series of RMSDs

5 of CNTL and CNTL_MOD have similar variations except for a slight phase shift, whereas that of REDIST shows a comparatively smaller increase in the RMSD in the summer. Specifically, the maximum RMSD of CNTL is 200.61 in mid-July and that of CNTL_MOD is 192.19 early in July, but that of REDIST is 127.32 at the beginning of June. Thus, REDIST is better than CNTL in simulating surface CO_2 fluxes in Asia in summer.

10 REDIST clearly outperforms CNTL and CNTL_MOD in summer, and an overall improvement is also observed from the comparison of the three experiments. The PC increases and the magnitudes of BIAS and RMSD decrease in REDIST compared to CNTL and CNTL_MOD. This implies that merely redistributing current observation sites in Asia could have more benefits in optimizing surface CO_2 fluxes. This result seems to be somewhat attributable to the fact that most observation sites in Asia in the NOAA

15 observation network of CT2013B are located in mid-latitudes (~35–45 ° N).

Furthermore, CNTL and CNTL_MOD are not much different in simulating surface CO_2 fluxes, which implies that the selection strategy of observation height in making hypothetical observations does not greatly affect the evaluation of the various observation networks. The real height information of the NOAA observation network in CNTL is therefore used for existing observation sites in Asia, and the

20 observation height of additional hypothetical sites is set to 5 meters above the model topography in the experiments.

3.2. Effect of an observation network with extra observation sites added randomly

Figure 5 presents the time series of the three-week moving average of PC, BIAS, and RMSD for

25 surface CO_2 fluxes from the CNTL, ADD, and ALL experiments, which clearly show the effect of randomly added observation sites. The decreases in the PC in the middle of April and in late July and August in CNTL do not appear in ADD and ALL (Fig. 5a). In particular, ALL maintains PC close to 1

during the experimental period. Although keeping the observation network as ALL is difficult in reality, this result demonstrates the impact of holding many observation sites in Asia. The minimum of the PC of ADD is 0.962, which is higher than that of CNTL (0.919), implying that adding extra observation sites in Asia could increase the stability in simulating surface CO_2 fluxes.

5   Compared to the BIAS of CNTL with high variability, the BIAS of ADD decreased by approximately 50% compared to that of CNTL and the absolute value of the maximum BIAS in ADD is 7.45 (Fig. 5b). Although ADD shows slightly higher BIAS than CNTL during the first two months, the time series of BIAS in ADD remains close to zero during the simulation period. The BIAS of ALL is the closest to 0 compared to those of CNTL and ADD throughout the experimental period.

10   In terms of the RMSD, the three experiments show increasing trends in the summer compared to other seasons (Fig. 5c), which is similar to the previous random redistribution experiments in Sect. 3.1. However, the RMSDs of ADD and ALL with more observation sites generally remain low during the simulation period. Specifically, compared to other seasons, the RMSD of CNTL in the summer increases by approximately three times and shows a four-fold increase in late July, rising to 200.61. Except in

15   summer, the time series of RMSD of ADD is similar to or slightly lower than that of CNTL. In summer, the maximum RMSD of ADD is reduced to 109.18, maintaining lower values during the summer and not showing any sudden increase. ALL has the minimum RMSD among the three experiments throughout the simulation period, and reaches a maximum of only 34.37 in early July. Since this number does not exceed the minimums of CNTL and ADD, the ALL experiment can be regarded as the best observation

20   network. This suggests that an accurate and stable optimization of surface CO_2 fluxes in Asia is possible if CO_2 observation sites are sufficient.

      The result of the observation network experiments with randomly added extra observation sites (i.e., ADD) also implies that the seven observation sites in Asia described in CT2013B do not seem to be sufficient to fully optimize the surface CO_2 fluxes in the region. Although the ADD experiment with 10

25   randomly added extra observation sites shows an improvement in optimization, more observation sites are necessary for optimizing surface CO_2 fluxes in Asia, considering the result of the ALL experiment. Moreover, the simulation result of the ADD experiment does not much outperform that of the REDIST experiment, although more observations were used. This implies that further consideration is required

when adding observation sites to the existing observation network. Thus, rather than just adding observation sites randomly, selecting and adding more influential observation sites for Asia is crucial to construct an efficient surface CO_2 observation network.

3.3. Effect of an observation network with extra observation sites added using self-sensitivity and ecoregion information

Considering the simulation results of Sect. 3.2, the addition of extra observation sites to the existing observation sites could improve the performance in simulating surface CO_2 fluxes in Asia. In particular, the ALL experiment, which added many observation sites enabled in the CT2013B framework, shows a high level of reproducibility of TRUE. However, adding more than 900 observation sites in Asia does not seem to be possible in real situations. Moreover, the expected effect from the extra observation sites may not be effective if the additional observations are not influential. Thus, the efficient selection and supplementation of observation sites is inevitable considering these constraints under realistic conditions.

In this study, self-sensitivity information obtained from the ALL experiment and ecoregion information used in CT2013B were used as additional strategies for the purpose of adding possible efficient observation sites in Asia. Since the self-sensitivity is the metric showing the impact of each observation site for the model simulation results, as stated in Sect. 2.2, it can be used as a strategy for selecting potential observation sites. In addition, the proportion of each ecoregion in the Asia domain can also be utilized as a strategy in choosing observation sites, as the calculation of surface carbon fluxes is based on the scaling factor for each ecoregion in CT2013B, and the scaling factor updated in the data assimilation process has the possibility to be more affected by the observation sites located in the same ecoregion (CarbonTracker Documentation CT2013B Release, 2015).

Figure 6 shows the spatial distribution of self-sensitivity from the ALL experiment. Although the self-sensitivity of each observation site varies from the others, four influential regions with high sensitivities are located in western Siberia, the southern part of the Tibetan Plateau, and southeastern and northeastern Asia. The highest (lowest) self-sensitivity of the hypothetical observation sites is 4.02% (0.04%). Thus, the likelihood of using observations located in the aforementioned four regions increases when considering the self-sensitivity as the selection strategy. In contrast, the observation sites located in

southwestern Asia and eastern Siberia are rarely chosen for the optimization due to the low value of self-sensitivity.

The self-sensitivity used for the SS and ECOSS experiments is the pure self-sensitivity without considering the number of assimilated observations. The 10 observation sites of the SS experiment were selected by employing self-sensitivity from the numerical order (highest first) and following the addition criteria (i.e., 1000 km distance between sites and observation height 5 meters above the model topography) used in Sect. 2.3. For the ECOSS experiment, the proportions of ecoregions in the Asia verification domain were calculated from the model grid-points. Following this, the observation sites were selected from the order of principal ecoregions with self-sensitivity information. Specifically, the land ecoregion information, omitting that of the oceans, was utilized for the selection criteria as the land in the northern hemisphere is crucial for the global carbon exchange. Table 3 displays the proportions of ecoregions in the Asia verification domain and the distribution of observation sites in SS and ECOSS. As the ecoregions with 115 and 137 indices constitute relatively large proportions of the ecoregions in Asia (Table 3), two observation sites were assigned for each of these two ecoregions. The other ecoregions have one observation site per ecoregion. When selecting the aforementioned two and one observation sites in the ecoregions, the observation sites with the highest self-sensitivities were selected. The observation sites of SS are mostly located in ecoregions that constitute lower proportions compared to those of ECOSS because the self-sensitivity is generally inversely proportional to the number of assimilated observations, as shown in Kim et al. (2014a, 2017).

The time series of the three-week moving average of PC, BIAS, and RMSD of the simulated surface CO_2 fluxes for the ADD, SS, and ECOSS experiments are shown in Fig. 7, which shows the impact of additional observation sites considering self-sensitivity information. The SS and ECOSS experiments show higher PC compared with ADD, except that the PC of SS is lower than that of ADD in late April and mid-August. In particular, the PC of ECOSS is superior to that of ADD throughout the experimental period and is more stable than that of SS. This result implies that the impact of extra observation sites added from self-sensitivity and ecoregion information is greater in optimizing surface CO_2 fluxes in Asia than that of randomly added observation sites.

However, the BIAS of SS shows a sudden increase in early July, with a maximum positive BIAS of 21.79 (Fig. 7b). Although the BIAS of ECOSS is generally closer to 0 than that of ADD, except in July, ECOSS shows the maximum negative BIAS of -15.78 in late July. These tendencies suggest that the DA method that optimizes parameters such as the scaling factor used in CT2013B may occasionally have

5   trouble in optimizing surface CO_2 fluxes when using limited observation sites for a larger area.

Nevertheless, the ECOSS experiment that considered both self-sensitivity and ecoregion information maintains lower RMSD than the ADD experiment over the experimental period. Additionally, the RMSD of SS is lower than that of ADD, except in the period from April to late-August. This is in contrast to the ADD experiment, which is mainly better than CNTL in summer, as shown in Fig. 5. Thus, in contrast to

10   ADD, the SS and ECOSS experiments demonstrate improvement in the other seasons except summer.

The increased RMSD of SS during the spring-summer period compared to that of ADD seems to be related to the DA method used in CT2013B. As most observation sites added in SS are located in the ecoregions with relatively small proportions of the Asia domain (Table 3), they may have disadvantages in optimizing the scaling factor of major ecoregions. This is somewhat relevant to the distribution of

15   observation sites in the ALL experiment, which has observation sites at 2° intervals, consequently leading to the uneven distribution of observation sites (i.e., major ecoregions with more observation sites and minor ecoregions with fewer observation sites) in Asia. As the self-sensitivity generally has an inverse relationship with the number of assimilated observations, the self-sensitivities of major ecoregions are typically lower than those of minor ecoregions, as shown in Table 4.

20   The simulation results of SS and ECOSS confirm that influential observation sites for optimizing surface CO_2 fluxes in Asia certainly exist, and the self-sensitivity information could be used for designing the observation network. The ECOSS experiment especially, which considers both ecoregion information and self-sensitivity, shows a better performance compared to the SS experiment, which suggests that considering characteristics of the specific model and data assimilation configurations can also contribute

25   to the improvement in optimization. This further implies that an observation network based on the self-sensitivity and ecoregion information could be better for optimizing surface CO_2 fluxes in Asia than that based on randomly added observation sites, though the same number of observations are used.

Atmospheric
Chemistry
and Physics
Discussions

3.4. Effect of an observation network with extra observation sites added using normalized self-sensitivity and ecoregion information

As stated in Sect. 3.3, using the pure self-sensitivities acquired from the ALL experiment for observation network studies could be inappropriate in certain occasions because they were derived from an uneven distribution of observation sites. Thus, self-sensitivity could be normalized (Eq. (15)) and used for the selection of observation sites. Table 5 shows the information for observation sites in the NSS, NECOSS1, and NECOSS2 experiments that used the normalized self-sensitivities as the selection strategy. The observation sites of the NSS experiment are located only in the 115 and 137 ecoregions. This is because they have higher normalized sensitivities than other regions as they constitute large proportions of the ecoregions of Asia, as shown in Table 3. Additionally, the NECOSS1 and NECOSS2 experiments were conducted to examine the impact of additional observation sites depending on the choice of ecoregion. For the NECOSS1 experiment, two observation sites were added to the 115 and 137 ecoregions and one observation site was allocated to the other six ecoregions. In contrast, the NECOSS2 experiment allotted one observation site to each ecoregion. The observation sites in NECOSS1 and NECOSS2 in the ecoregions were selected by the order of highest normalized sensitivities in each ecoregion.

Figure 8 shows the time series of the three-week moving average of PC, BIAS, and RMSD of the simulated surface CO_2 fluxes for the ADD, NSS, NECOSS1, and NECOSS2 experiments, which shows the impact of using normalized self-sensitivities for the selection of additional observation sites. For the PC, all the experiments using normalized self-sensitivities (i.e., NSS, NECOSS1, and NECOSS2) show higher PC than the ADD experiment for most of the time (Fig. 8a). In particular, the PC of NSS is always higher than the PC of SS that showed temporarily lower PC compared to ADD from late April to mid-August. Furthermore, the NECOSS1 and NECOSS2 experiments that also considered ecoregion information perform better than the NSS experiment without ecoregion information.

Regarding BIAS, the experiments using the normalized self-sensitivities show a strong negative BIAS in mid- and late July (Fig. 8b). Although such tendencies are similar to that of ECOSS shown in Fig. 7b, the maximum negative BIAS of NSS, NECOSS1, and NECOSS2 are -14.40, -12.23, and -11.45,

respectively, which is comparatively smaller than that of ECOSS. Such an abrupt increase in BIAS could be associated with the sudden transition of surface carbon sources and sinks during summer.

The NSS, NECOSS1, and NECOSS2 experiments show lower RMSDs compared to the ADD experiment (Fig. 8c). The RMSD of NSS is lower than that of SS for most of the time, and this is in contrast to SS that showed a degradation in summer and little improvement in other seasons compared to ADD in Fig. 7c. Moreover, the NECOSS1 and NECOSS2 experiments that additionally considered the ecoregion information demonstrate a further reduction in RMSD, especially in summer. The NECOSS1 and NECOSS2 experiments have a slightly lower RMSD than ECOSS that considered pure self-sensitivities and ecoregion information. The NECOSS1 and NECOSS2 experiments do not show significant differences due to minor differences in the choice of observation sites.

The simulation results using the normalized self-sensitivities reconfirm that the self-sensitivity information could be used in designing the observation network. By considering the DA method of CT2013B that optimizes scaling factors assigned in ecoregions, the experiments using normalized self-sensitivities could make simulations better than those using pure self-sensitivity. In addition, the additional consideration of ecoregion in the experiments using normalized self-sensitivities also contributes to improvements, which implies that the model's characteristics, such as ecoregion information, could also be one of the factors to be used in designing the surface CO_2 observation network.

3.5. Horizontal distributions of RMSD and uncertainty reduction

Figure 9 shows the spatial distribution of the average of weekly RMSD calculated from the surface CO_2 fluxes in Asia. The CNTL shows the highest RMSD among the experiments, with peaks mainly located in the Siberian area (Fig. 9a). The REDIST experiment shows a decrease in the high RMSD of the Siberian area shown in CNTL, but the RMSDs of eastern China and the southeastern part of the Tibetan Plateau (the Indochina Peninsula) slightly increase, and the RMSDs of northern India and the northeastern part of Asia remain nearly unchanged compared to CNTL (Fig. 9b). The distribution of RMSD in the ADD experiment is fairly similar to that of REDIST, except for the decrease of RMSD near the Tibetan Plateau and in southeastern Asia (Fig. 9c). Such a spatial distribution of RMSD in the ADD

experiment implies the need for supplementing observation sites efficiently. Figure 9d clearly shows the reduction in RMSD of northern India and the southeastern region of the Tibetan Plateau in the SS experiment compared to the REDIST and ADD experiments. This proves the impact of considering self-sensitivity information for observation network studies. However, the performance of the SS experiment

5   on some Siberian inland areas is poorer than those of the REDIST and ADD experiments, due to the relative absence of observation sites for that region. The ECOSS experiment using the ecoregion information shows comparatively lower RMSD in the Asia domain, except for the southeastern part of the Tibetan Plateau and northeastern Asia (Fig. 9e). The RMSD distribution of the NSS experiment confirms that the RMSD of the Siberian area is much reduced compared to that of the SS experiment,

10 though its overall pattern is similar (Fig. 9f). The RMSDs of the NECOSS1 and NECOSS2 experiments are analogous to that of the ECOSS experiment (Fig. 9g). This can be attributed to the fact that most observation sites in those three experiments are identical (Tables 4 and 5). The simulated RMSD of the ALL experiment is the lowest in most of the domain among all sensitivity experiments (Fig. 9i). Such simulation results reconfirm that the observation network in Asia needs to be organized in a more efficient

15 way to gain better optimization results of surface CO_2 fluxes.

Figure 10 shows the UR derived from the experiments, which corresponds with the previous results. Compared to the CNTL experiment, the uncertainty of the REDIST experiment is much reduced in the Siberian area, but the impact of REDIST is low below 50° N (Fig. 10a). Such a result seems to be related with the high UR values in that region in CNTL, because most observation sites in CNTL are located

20 from 30° to 45° N. The ADD experiment with randomly added sites demonstrates slight increases in UR for the inland Siberian area and the nearby areas of the Tibetan Plateau, including China and India (Fig. 10b). However, the UR in the Asian mid-latitudes is still lower than that in other Asian regions. Although the SS and ECOSS experiments have the same number of observation sites compared with the ADD experiment, the overall UR in the Asia domain in SS and ECOSS is higher than that of ADD (Figs. 10b,

25 c, and d). The uncertainty in the SS experiment, which has comparatively more observation sites in India and southeastern Asia, is clearly reduced for that area. In contrast, the ECOSS experiment retaining comparatively more observation sites in the inland areas of Asia shows higher UR in the land areas, although UR in India and southeastern Asia is lower than that in the SS experiment. The experiments

Atmospheric
Chemistry
and Physics
Discussions
EGU
Open Access

using normalized self-sensitivities generally show distinct uncertainty reductions in inland Asia, although the UR of India and southeastern Asia in NSS is slightly lower than that of SS (Fig. 10e). This is because the observation sites of NSS are located only in the 115 and 137 ecoregions. Although the UR distributions of the NECOSS1 and NECOSS2 experiments are generally similar to those of the ECOSS experiment, the uncertainties in India and southeastern Asia decrease further in NECOSS1 and NECOSS2 (Figs. 10f and g). The UR of the ALL experiment increases compared to those of other experiments as a number of observation sites in ALL sufficiently cover the Asian domain (Fig. 10h).

Table 6 summarizes the overall scores of the simulations conducted in this study. The CNTL (ALL) experiment shows the lowest (highest) skill score among the simulations. The skill scores of other experiments range between these. The statistics shown in Table 6 reconfirm the impacts of redistributing current observation sites and adding extra observation sites discussed in this study. Firstly, the height specification for hypothetical observations does not seem to be very influential for OSSE results as only small differences were observed between the results of CNTL and CNTL_MOD. The impact of redistribution is noticeable because the performance of the REDIST experiment was generally better than that of the CNTL experiment. Moreover, the comparison between ADD, SS, and ECOSS reaffirms that adding more observation sites to the existing sites is effective in optimizing surface CO_2 fluxes, and the addition strategy needs to be more effective to have better optimization results for surface CO_2 fluxes. Moreover, the NSS, NECOSS1, and NECOSS2 experiments that used both normalized self-sensitivities and ecoregion information show that the normalized self-sensitivity and configuration of the data assimilation and model can be utilized as appropriate strategies in designing an observation network that enhances simulation results. The simulation result of the ALL experiment seems to suggest a possible limit of the improvement when using the DA method in CT2013B.

4. Conclusions

In this study, observation system simulation experiments using hypothetical observations were conducted to investigate the potential for an effective observation network for optimizing surface CO_2 fluxes in Asia. Several experiments, including redistributing existing stations and adding observation stations to the existing observation network, were conducted to assess the performance of the current

observation network and the impact of additional observation sites. For the addition experiment, random addition and addition strategies based on self-sensitivities, normalized self-sensitivities, and ecoregion information were tested and compared. The performance of each observation network was evaluated from statistics calculated from simulated surface CO_2 fluxes and the uncertainty reduction.

5   The results indicate that further optimization of the surface CO_2 fluxes in Asia could be made by redistributing existing observation sites, given that the RMSD of the redistributed experiment was reduced by 12.8% compared to the experiment using the existing observation network (i.e., CNTL). The RMSD of the random addition experiment was reduced by 21.9% compared to CNTL. Although the experiment based on only self-sensitivity information was not better than that based on randomly added observation

10   sites, the experiment based on both self-sensitivity and ecoregion information reduced the RMSD by 35.2% compared to that of CNTL. Moreover, the experiment based on both normalized self-sensitivity and ecoregion information further reduced the RMSD by approximately 40% compared to that of CNTL. Thus, the normalized self-sensitivity and ecoregion information could be used as strategies to select observation sites to construct the surface CO_2 observation network.

15   Although the simulation results showed an improvement in performance, the results also suggested that adding 10 extra observation sites in Asia may not be sufficient to fully optimize surface CO_2 fluxes, and more observation sites are required. Reliable observation data from some satellite sensors could supplement the model simulations on the basis of continuous surface observation sites.

       This study suggests a method to design and evaluate the observation network to optimize surface CO_2

20   fluxes at the continental scale without a myriad of simulations (iterations) of the genetic algorithm or the incremental optimization used in previous studies. Thus, this approach could constitute a practical method to conduct such simulations with relatively limited computer resources. The observation network design method in this study could also be used to design an observation network to optimize global surface CO_2 fluxes.

Author contribution

Hyun Mee Kim proposed the main scientific ideas and Jun Park contributed the supplementary ideas during the process. Jun Park ran the observation system simulation experiments using CarbonTracker. Jun Park and Hyun Mee Kim analyzed the simulation results and completed the manuscript.

References

Byrne, B., Jones, D. B. A., Strong, K., Zeng, Z. C., Deng, F. and Liu, J.: Sensitivity of CO_2 surface flux constraints to observational coverage, J. Geophys. Res. Atmos., 122(12), 6672–6694, doi:10.1002/2016JD026164, 2017.

5 Boden, T., Marland, G., and Andres, R.: Global, regional, and national fossil-fuel CO_2 emissions, Carbon Dioxide Information Analysis Center, Oak Ridge National Laboratory, US Department of Energy, Oak Ridge, TN, USA, 10, doi:10.3334/CDIAC/00001_V2010, 2010.

CarbonTracker Documentation CT2013B Release, CarbonTracker Team, available at: https://www.esrl.noaa.gov/gmd/ccgg/carbontracker/CT2013B/CT2013B_doc.php (last access: January

10 2019), 2015.

Cardinali, C., Pezzulli, S. and Andersson, E.: Influence-matrix diagnostic of a data assimilation system, Q. J. R. Meteorol. Soc., 130(603 PART B), 2767–2786, doi:10.1256/qj.03.205, 2004.

Cheng, Y. L., Aa, X. Q., Yun, F. H., Zhou, L. X., Liu, L. X., Fang, S. X. and Xu, L.: Simulation of CO_2 variations at Chinese background atmospheric monitoring stations between 2000 and 2009: Applying a

15 CarbonTracker model, Chinese Sci. Bull., 58(32), 3986–3993, doi:10.1007/s11434-013-5895-y, 2013.

Cheng, S., Zhou, L., Tans, P. P., An, X. and Liu, Y.: Comparison of atmospheric CO_2 mole fractions and source–sink characteristics at four WMO/GAW stations in China, Atmos. Environ., 180(March), 216–225, doi:10.1016/j.atmosenv.2018.03.010, 2018.

Chevallier, F., Engelen, R. J., Carouge, C., Conway, T. J., Peylin, P., Pickett-Heaps, C., Ramonet, M.,

20 Rayner, P. J. and Xueref-Remy, I.: AIRS-based versus flask-based estimation of carbon surface fluxes, J. Geophys. Res. Atmos., 114(20), 1–9, doi:10.1029/2009JDO12311, 2009a.

Chevallier, F., Maksyutov, S., Bousquet, P., Bréon, F. M., Saito, R., Yoshida, Y. and Yokota, T.: On the accuracy of the CO_2 surface fluxes to be estimated from the GOSAT observations, Geophys. Res. Lett., 36(19), 1–5, doi:10.1029/2009GL040108, 2009b.

25 Chevallier, F., Ciais, P., Conway, T. J., Aalto, T., Anderson, B. E., Bousquet, P., Brunke, E. G., Ciattaglia, L., Esaki, Y., Fröhlich, M., Gomez, A., Gomez-Pelaez, A. J., Haszpra, L., Krummel, P. B., Langenfelds, R. L., Leuenberger, M., MacHida, T., Maignan, F., Matsueda, H., Morguí, J. A., Mukai, H., Nakazawa, T., Peylin, P., Ramonet, M., Rivier, L., Sawa, Y., Schmidt, M., Steele, L. P., Vay, S. A., Vermeulen, A.

T., Wofsy, S. and Worthy, D.: CO_2 surface fluxes at grid point scale estimated from a global 21 year reanalysis of atmospheric measurements, J. Geophys. Res. Atmos., 115(21), 1–17, doi:10.1029/2010JD013887, 2010.

Enting, I. G.: Inverse problems in atmospheric constituent transport, Cambridge University Press., 2002.

5   European Commission: Joint Research Centre (JRC)/Netherlands Environmental Assessment Agency (PBL): Emission Database for Global Atmospheric Research (EDGAR), release version 4.0, 2009.

Evensen, G.: Sequential data assimilation with a nonlinear quasi-geostrophic model using Monte Carlo methods to forecast error statistics, J. Geophys. Res. Oceans, 99(C5), 10143, doi:10.1029/94JC00572, 1994.

10 Feng, L., Palmer, P. I., Bösch, H. and Dance, S.: Estimating surface CO_2 fluxes from space-borne CO_2 dry air mole fraction observations using an ensemble Kalman Filter, Atmos. Chem. Phys., 9, 2619–2633, doi:10.5194/acp-9-2619-2009, 2009.

Feng, L., Palmer, P. I., Parker, R. J., Deutscher, N. M., Feist, D. G., Kivi, R., Morino, I. and Sussmann, R.: Estimates of European uptake of CO_2 inferred from GOSAT XCO_2 retrievals: Sensitivity to 15 measurement bias inside and outside Europe, Atmos. Chem. Phys., 16(3), 1289–1302, doi:10.5194/acp-16-1289-2016, 2016.

Fischer, M. L., Parazoo, N., Brophy, K., Cui, X., Jeong, S., Liu, J., Keeling, R., Taylor, T. E., Gurney, K., Oda, T. and Graven, H.: Simulating estimation of California fossil fuel and biosphere carbon dioxide exchanges combining in situ tower and satellite column observations, J. Geophys. Res. Atmos., 122(6), 20 3653–3671, doi:10.1002/2016JD025617, 2017.

Gurney, K. R., Law, R. M., Denning, A. S., Rayner, P. J., Baker, D., Bousquet, P., Bruhwiler, L., Chen, Y.-H., Ciais, P., Fan, S., Fung, I. Y., Gloor, M., Heimann, M., Higuchi, K., John, J., Maki, T., Maksyutov, S., Masarie, K., Peylin, P., Prather, M., Pak, B. C., Randerson, J., Sarmiento, J., Taguchi, S., Takahashi, T. and Yuen, C.-W.: Towards robust regional estimates of CO_2 sources and sinks using atmospheric 25 transport models, Nature, 415(6872), 626–630, doi:10.1038/415626a, 2002.

Hayes, D. J., McGuire, A. D., Kicklighter, D. W., Gurney, K. R., Burnside, T. J. and Melillo, J. M.: Is the northern high-latitude land-based CO_2 sink weakening?, Global Biogeochem. Cycles, 25(3), 1–14, doi:10.1029/2010GB003813, 2011.

Houghton, R. A., Butman, D., Bunn, A. G., Krankina, O. N., Schlesinger, P. and Stone, T. A.: Mapping Russian forest biomass with data from satellites and forest inventories, Environ. Res. Lett., 2(4), doi:10.1088/1748-9326/2/4/045032, 2007.

Houtekamer, P. L. and Mitchell, H. L.: A Sequential Ensemble Kalman Filter for Atmospheric Data
5 Assimilation, Mon. Weather Rev., 129(1), 123–137, doi:10.1175/1520-0493(2001)129<0123:ASEKFF>2.0.CO;2, 2001.

Jacobson, A. R., Fletcher, S. E. M., Gruber, N., Sarmiento, J. L. and Gloor, M.: A joint atmosphere-ocean inversion for surface fluxes of carbon dioxide: 1. Methods and global-scale fluxes, Global Biogeochem. Cycles, 21(1), doi:10.1029/2005GB002556, 2007.

10 Kang, J.-S., Kalnay, E., Liu, J., Fung, I., Miyoshi, T. and Ide, K.: "Variable localization" in an ensemble Kalman filter: Application to the carbon cycle data assimilation, J. Geophys. Res. Atmos., 116(D9), D09110, doi:10.1029/2010JD014673, 2011.

Kang, J.-S., Kalnay, E., Miyoshi, T., Liu, J. and Fung, I.: Estimation of surface carbon fluxes with an advanced data assimilation methodology, J. Geophys. Res. Atmos., 117(D24),
15 doi:10.1029/2012JD018259, 2012.

Kim, H., Kim, H. M., Kim, J. and Cho, C.-H.: A Comparison of the Atmospheric CO_2 Concentrations Obtained by an Inverse Modeling System and Passenger Aircraft Based Measurement, Atmos., 26(3), 387-400, doi:10.14191/Atmos.2016.26.3.387, 2016. (in Korean with English abstract)

Kim, H., Kim, H. M., Cho, M., Park, J., and Kim, D.-H.: Development of the Aircraft CO_2 Measurement
20 Data Assimilation System to Improve the Estimation of Surface CO_2 Fluxes Using an Inverse Modeling System, Atmos., 28(2), 113-121, doi:10.14191/Atmos.2018.28.2.113, 2018a. (in Korean with English abstract)

Kim, H., Kim, H. M., Kim, J. and Cho, C.-H.: Effect of data assimilation parameters on the optimized surface CO_2 flux in Asia, Asia-Pacific J. Atmos. Sci., 54(1), 1–17, doi:10.1007/s13143-017-0049-9,
25 2018b.

Kim, J., Kim, H. M. and Cho, C. H.: Influence of CO_2 observations on the optimized CO_2 flux in an ensemble Kalman filter, Atmos. Chem. Phys., 14(24), 13515–13530, doi:10.5194/acp-14-13515-2014, 2014a.

Kim, J., Kim, H. M. and Cho, C. H.: The effect of optimization and the nesting domain on carbon flux analyses in Asia using a carbon tracking system based on the ensemble Kalman filter, Asia-Pacific J. Atmos. Sci., 50(3), 327–344, doi:10.1007/s13143-014-0020-y, 2014b.

Kim, J., Kim, H. M., Cho, C. H., Boo, K. O., Jacobson, A. R., Sasakawa, M., Machida, T., Arshinov, M.
5 and Fedoseev, N.: Impact of Siberian observations on the optimization of surface CO_2 flux, Atmos. Chem. Phys., 17(4), 2881–2899, doi:10.5194/acp-17-2881-2017, 2017.

Kim, J., Kim, H. M. and Cho, C.: Application of Carbon Tracking System based on Ensemble Kalman Filter on the Diagnosis of Carbon Cycle in Asia, Atmos., 22(4), 415–427, 2012. (in Korean with English abstract)

10 Kou, X., Tian, X., Zhang, M., Peng, Z. and Zhang, X.: Accounting for CO_2 Variability over East Asia with a Regional Joint Inversion System, J. Meteorol. Res., 31(5), 834-851, doi:10.1007/s13351-017-6149-8. 2017.

Krol, M., Houweling, S., Bregman, B., van den Broek, M., Segers, A., van Velthoven, P., Peters, W., Dentener, F. and Bergamaschi, P.: The two-way nested global chemistry-transport zoom model TM5:
15 algorithm and applications. Atmos. Chem. Phys., 5, 417-432. 2005.

Kurganova, I. N., Kudeyarov, V. N. and Lopes De Gerenyu, V. O.: Updated estimate of carbon balance on Russian territory, Tellus, Ser. B Chem. Phys. Meteorol., 62(5), 497–505, doi:10.1111/j.1600-0889.2010.00467.x, 2010.

Lacis, A. A., Schmidt, G. A., Rind, D. and Ruedy, R. A.: Atmospheric CO_2: Principal control knob
20 governing earth's temperature, Science, 330(6002), 356–359, doi:10.1126/science.1190653, 2010.

Le Quéré, C., Andrew, R. M., Friedlingstein, P., Sitch, S., Pongratz, J., Manning, A. C., Korsbakken, J. I., Peters, G. P., Canadell, J. G., Jackson, R. B., Boden, T. A., Tans, P. P., Andrews, O. D., Arora, V. K., Bakker, D. C. E., Barbero, L., Becker, M., Betts, R. A., Bopp, L., Chevallier, F., Chini, L. P., Ciais, P., Cosca, C. E., Cross, J., Currie, K., Gasser, T., Harris, I., Hauck, J., Haverd, V., Houghton, R. A., Hunt,
25 C. W., Hurtt, G., Ilyina, T., Jain, A. K., Kato, E., Kautz, M., Keeling, R. F., Klein Goldewijk, K., Körtzinger, A., Landschützer, P., Lefèvre, N., Lenton, A., Lienert, S., Lima, I, Lombardozzi, D., Metzl, N., Millero, F., Monteiro, P. M. S., Munro, D. R., Nabel, J. E. M. S., Nakaoka, S.-I., Nojiri, Y., Padin, X. A., Peregon, A., Pfeil, B., Pierrot, D., Poulter, B., Rehder, G., Reimer, J., Rödenbeck, C., Schwinger, J.,

Séférian, R., Skjelvan, I., Stocker, B. D., Tian, H., Tilbrook, B., Tubiello, F. N., Van Der Laan-Luijkx, I. T., Van Der Werf, G. R., Van Heuven, S., Viovy, N., Vuichard, N., Walker, A. P., Watson, A. J., Wiltshire, A. J., Zaehle, S. and Zhu, D.: Global Carbon Budget 2017, Earth Syst. Sci. Data, 10, 405–448, doi:10.5194/essd-10-405-2018, 2018.

5   Liu, J., Kalnay, E., Miyoshi, T., and Cardinali, C.: Analysis sensitivity calculation in an ensemble Kalman filter, Q. J. R. Meteorol. Soc., 135, 1842-1851, doi:10.1002/qj.511, 2009.

Lucas, D. D., Yver Kwok, C., Cameron-Smith, P., Graven, H., Bergmann, D., Guilderson, T. P., Weiss, R. and Keeling, R.: Designing optimal greenhouse gas observing networks that consider performance and cost, Geosci. Instrumentation, Methods Data Syst., 4(1), 121–137, doi:10.5194/gi-4-121-2015, 2015.

10   Maksyutov, S., Takagi, H., Valsala, V. K., Saito, M., Oda, T., Saeki, T., Belikov, D. A., Saito, R., Ito, A., Yoshida, Y., Morino, I., Uchino, O., Andres, R. J. and Yokota, T.: Regional CO_2 flux estimates for 2009-2010 based on GOSAT and ground-based CO_2 observations, Atmos. Chem. Phys., 13(18), 9351–9373, doi:10.5194/acp-13-9351-2013, 2013.

Meirink, J. F., Bergamaschi, P. and Krol, M. C.: Four-dimensional variational data assimilation for
15   inverse modelling of atmospheric methane emissions: Method and comparison with synthesis inversion, Atmos. Chem. Phys., 8(21), 6341–6353, doi:10.5194/acp-8-6341-2008, 2008.

Nickless, A., Ziehn, T., Rayner, P. J., Scholes, R. J. and Engelbrecht, F.: Greenhouse gas network design using backward Lagrangian particle dispersion modelling - Part 2: Sensitivity analyses and South African test case, Atmos. Chem. Phys., 15(4), 2051–2069, doi:10.5194/acp-15-2051-2015, 2015.

20   Olson, J., Watts, J., and Allsion, L.: Major World Ecosystem Complexes Ranked by Carbon in Live Vegetation: a Database, Tech. rep., Carbon Dioxide Information Analysis Center, U.S. Department of Energy, Oak Ridge National Laboratory, Oak Ridge, TN, USA, doi:10.3334/CDIAC/lue.ndp017, 1992.

Peters, W., Krol, M. C., Dlugokencky, E. J., Dentener, F. J., Bergamaschi, P., Dutton, G., Velthoven, P. v., Miller, J. B., Bruhwiler, L. and Tans, P. P.: Toward regional-scale modeling using the two-way nested
25   global model TM5: Characterization of transport using SF6, J. Geophys. Res. Atmos., 109(19), doi:10.1029/2004JD005020, 2004.

Peters, W., Miller, J. B., Whitaker, J., Denning, A. S., Hirsch, A., Krol, M. C., Zupanski, D., Bruhwiler, L. and Tans, P. P.: An ensemble data assimilation system to estimate CO_2 surface fluxes from atmospheric trace gas observations, J. Geophys. Res. Atmos., 110(D24), D24304, doi:10.1029/2005JD006157, 2005.

Peters, W., Jacobson, A. R., Sweeney, C., Andrews, A. E., Conway, T. J., Masarie, K., Miller, J. B.,
5 Bruhwiler, L. M. P., Petron, G., Hirsch, A. I., Worthy, D. E. J., van der Werf, G. R., Randerson, J. T., Wennberg, P. O., Krol, M. C. and Tans, P. P.: An atmospheric perspective on North American carbon dioxide exchange: CarbonTracker, Proc. Natl. Acad. Sci., 104(48), 18925–18930, doi:10.1073/pnas.0708986104, 2007.

Peters, W., Krol, M. C., van der Werf, G. R., Houweling, S., Jones, C. D., Hughes, J., Schaefer, K.,
10 Masarie, K. A., Jacobson, A. R., Miller, J. B., Cho, C. H., Ramonet, M., Schmidt, M., Ciattaglia, L., Apadula, F., Heltai, D., Meinhardt, F., di Sarra, A. G., Piacentino, S., Sferlazzo, D., Aalto, T., Hatakka, J., StröM, J., Haszpra, L., Meijer, H. A. J., van Der Laan, S., Neubert, R. E. M., Jordan, A., Rodó, X., Morguí, J. A., Vermeulen, A. T., Popa, E., Rozanski, K., Zimnoch, M., Manning, A. C., Leuenberger, M., Uglietti, C., Dolman, A. J., Ciais, P., Heimann, M. and Tans, P.: Seven years of recent European net
15 terrestrial carbon dioxide exchange constrained by atmospheric observations, Glob. Chang. Biol., 16(4), 1317–1337, doi:10.1111/j.1365-2486.2009.02078.x, 2010.

Peylin, P., Law, R. M., Gurney, K. R., Chevallier, F., Jacobson, A. R., Maki, T., Niwa, Y., Patra, P. K., Peters, W., Rayner, P. J., Rödenbeck, C., Van Der Laan-Luijkx, I. T. and Zhang, X.: Global atmospheric carbon budget: Results from an ensemble of atmospheric CO_2 inversions, Biogeosciences, 10(10), 6699–
20 6720, doi:10.5194/bg-10-6699-2013, 2013.

Reuter, M., Buchwitz, M., Hilker, M., Heymann, J., Schneising, O., Pillai, D., Bovensmann, H., Burrows, J. P., Bösch, H., Parker, R., Butz, A., Hasekamp, O., O'Dell, C. W., Yoshida, Y., Gerbig, C., Nehrkorn, T., Deutscher, N. M., Warneke, T., Notholt, J., Hase, F., Kivi, R., Sussmann, R., Machida, T., Matsueda, H. and Sawa, Y.: Satellite-inferred European carbon sink larger than expected, Atmos. Chem. Phys.,
25 14(24), 13739–13753, doi:10.5194/acp-14-13739-2014, 2014.

Saeki, T., Maksyutov, S., Sasakawa, M., Machida, T., Arshinov, M., Tans, P., Conway, T. J., Saito, M., Valsala, V., Oda, T., Andres, R. J. and Belikov, D.: Carbon flux estimation for siberia by inverse modeling

Atmospheric
Chemistry
and Physics
Discussions

Open Access

EGU

constrained by aircraft and tower CO_2 measurements, J. Geophys. Res. Atmos., 118(2), 1100–1122, doi:10.1002/jgrd.50127, 2013.

Sasakawa, M., Shimoyama, K., Machida, T., Tsuda, N., Suto, H., Arshinov, M., Davydov, D., Fofonov, A., Krasnov, O., Saeki, T., Koyama, Y. and Maksyutov, S.: Continuous measurements of methane from a tower network over Siberia, Tellus, Ser. B Chem. Phys. Meteorol., 62(5), 403–416, doi:10.1111/j.1600-0889.2010.00494.x, 2010.

Sasakawa, M., Machida, T., Tsuda, N., Arshinov, M., Davydov, D., Fofonov, A. and Krasnov, O.: Aircraft and tower measurements of CO_2 concentration in the planetary boundary layer and the lower free troposphere over southern taiga in West Siberia: Long-term records from 2002 to 2011, J. Geophys. Res. Atmos., 118(16), 9489–9498, doi:10.1002/jgrd.50755, 2013.

Schepaschenko, D., McCallum, I., Shvidenko, A., Fritz, S., Kraxner, F. and Obersteiner, M.: A new hybrid land cover dataset for Russia: A methodology for integrating statistics, remote sensing and in situ information, J. Land Use Sci., 6(4), 245–259, doi:10.1080/1747423X.2010.511681, 2011.

Schulze, E. D., Lloyd, J., Kelliher, F. M., Wirth, C., Rebmann, C., Luhker, B., Mund, M., Knohl, A., Milyukova, I. M., Schulze, W., Ziegler, W., Varlagin, A. B., Sogachev, A. F., Valentini, R., Dore, S., Grigoriev, S., Kolle, O., Panfyorov, M. I., Tchebakova, N. and Vygodskaya, N. N.: Productivity of forests in the eurosiberian boreal region and their potential to act as a carbon sink - a synthesis, Glob. Chang. Biol., 5(6), 703–722, doi:10.1046/j.1365-2486.1999.00266.x, 1999.

Siewert M. B., Hanisch J., Weiss N., Kuhry P., Maximov T. C., and H. G.: Comparing carbon storage of Siberian tundra and taiga permafrost ecosystems at very high spatial resolution, J. Geophys. Res. Biogeosciences, 120, 1973–1994, doi:10.1002/ 2015JG002999, 2015.

Tamocai, C., Canadell, J. G., Schuur, E. A. G., Kuhry, P., Mazhitova, G. and Zimov, S.: Soil organic carbon pools in the northern circumpolar permafrost region, Global Biogeochem. Cycles, 23(2), 1–11, doi:10.1029/2008GB003327, 2009.

van der Werf, G. R., Randerson, J. T., Giglio, L., Collatz, G. J., Kasibhatla, P. S. and Arellano, Avelino F., J.: Interannual variability in global biomass burning emissions from 1997 to 2004, Atmos. Chem. Phys., 6(11), 3423–3441, doi:10.5194/acpd-6-3175-2006, 2006.

van der Werf, G. R., Randerson, J. T., Giglio, L., Collatz, G. J., Mu, M., Kasibhatla, P. S., Morton, D. C., Defries, R. S., Jin, Y. and Van Leeuwen, T. T.: Global fire emissions and the contribution of deforestation, savanna, forest, agricultural, and peat fires (1997-2009), Atmos. Chem. Phys., 10(23), 11707–11735, doi:10.5194/acp-10-11707-2010, 2010.

Wang, Y., Broquet, G., Ciais, P., Chevallier, F., Vogel, F., Wu, L., Yin, Y., Wang, R. and Tao, S.: Potential of European $^{14}CO_2$ observation network to estimate the fossil fuel CO_2 emissions via atmospheric inversions, Atmos. Chem. Phys, 185194(July), 4229–4250, doi:10.5194/acp-18-4229-2018, 2018.

Whitaker, J. S. and Hamill, T. M.: Ensemble Data Assimilation without Perturbed Observations, Mon. Weather Rev., 130(7), 1913–1924, doi:10.1175/1520-0493(2002)130<1913:EDAWPO>2.0.CO;2, 2002.

Wu, K., Lauvaux, T., Davis, K. J., Deng, A., Lopez Coto, I., Gurney, K. R. and Patarasuk, R.: Joint inverse estimation of fossil fuel and biogenic CO_2 fluxes in an urban environment: An observing system simulation experiment to assess the impact of multiple uncertainties, Elem. Sci. Anthropocene, 6(1), 17, doi:10.1525/elementa.138, 2018.

Yang, E.-G., H. M. Kim, J. Kim, and Kay J. K.: Effect of observation network design on meteorological forecasts of Asian dust events, Monthly Weather Review, 142, 4679-4695, doi:10.1175/MWR-D-14-00080.1, 2014.

Ziehn, T., Nickless, A., Rayner, P. J., Law, R. M., Roff, G. and Fraser, P.: Greenhouse gas network design using backward Lagrangian particle dispersion modelling - Part 1: Methodology and Australian test case, Atmos. Chem. Phys., 14(17), 9363–9378, doi:10.5194/acp-14-9363-2014, 2014.

Ziehn, T., Law, R. M., Rayner, P. J. and Roff, G.: Designing optimal greenhouse gas monitoring networks for Australia, Geosci. Instrumentation, Methods Data Syst., 5(1), 1–15, doi:10.5194/gi-5-1-2016, 2016.

Table 1. The model configuration and a priori fluxes used in this study.

Prior Flux	Biosphere	Carnegie-Ames-Stanford Approach Global Fire Emission Database (CASA-GFED) v3.1 (van der Werf et al., 2006, 2010)
	Ocean	Jacobson et al. (2007)
	Fossil Fuel	CASA-GFED v3.1 (van der Werf et al., 2006, 2010)
	Fires	Carbon Dioxide Information and Analysis Center (CDIAC; Boden et al., 2010) and Emission Database for Global Atmospheric Research (EDGAR, European Commission, 2009) databases
Model	Transport Model 5 (TM5) using ERA-interim reanalysis	
Model Resolution	Domain 1(3°×2°)	Globe
	Domain 2(1°×1°)	Asia (12°S-70°N, 30°-168°E)

Table 2. Brief description of the experiments conducted in this study.

Exp. name	No. of stations	Description
CNTL	7	The control experiment that uses the observation site information in Asia of the existing NOAA observation network.
CNTL_MOD	7	The same as the CNTL except for modifying observation station height information for hypothetical observations.
REDIST	7	The experiment that redistributes 7 observations sites at random in Asia.
ADD	17	The experiment that added 10 observation sites at random to the existing NOAA observation network.
SS	17	The experiment that added 10 observation sites to the existing NOAA observation network with the self-sensitivity information.
ECOSS	17	The experiment that added 10 observation sites to the existing NOAA observation network with the self-sensitivity and ecoregion information (1-2 stations for each ecoregion)
NSS	17	The experiment that added 10 observation sites to the existing NOAA observation network with the normalized self-sensitivity information.
NECOSS1	17	The experiment that added 10 observation sites to the existing NOAA observation network with the normalized self-sensitivity and ecoregion information (1-2 stations for each ecoregion)
NECOSS2	17	The experiment that added 10 observation sites to the existing NOAA observation network with the normalized self-sensitivity and ecoregion information (1 station per ecoregion)
ALL	905	The experiment that added observation sites at horizontal 2° inter vals on land to the existing NOAA observation network.

Table 3. The proportion of the ecoregions in the Asia verification domain and the distribution of observation sites for the SS and ECOSS experiments.

Ecoregion Index	Count	Proportion (%)	SS	ECOSS
137	744	19.36		2
115	657	17.10		2
140	262	6.82		1
147	248	6.45		1
123	228	5.93		1
157	222	5.78		1
145	200	5.20		
117	150	3.90		1
118	122	3.17		
136	122	3.17		
121	95	2.47		
166	80	2.08		
135	62	1.61		
141	59	1.54		
143	58	1.51	1	
171	54	1.41		
125	45	1.17	1	
162	44	1.14		
122	42	1.09		
154	39	1.01	1	
155	37	0.96		
156	36	0.94		
124	35	0.91		
134	34	0.88		
116	33	0.86		
128	24	0.62	1	
138	19	0.49	1	
160	15	0.39		
146	12	0.31		
144	11	0.29	1	
139	10	0.26	1	
163	9	0.23	2	
152	8	0.21		
130	5	0.13	1	
133	5	0.13		
191	5	0.13		
193	4	0.10		
194	4	0.10		
197	3	0.08		
201	1	0.03		

Atmospheric
Chemistry
and Physics
Discussions

Table 4. The locations and self-sensitivities for the observation sites in the SS and ECOSS experiments.

SS				ECOSS			
Ecoregion Index	Lat	Lon	SS (%)	Ecoregion Index	Lat	Lon	SS (%)
138	26.5	96.5	4.02	137	26.5	92.5	0.87
163	4.5	114.5	3.83	137	28.5	118.5	0.65
163	-5.5	138.5	3.29	115	58.5	62.5	1.35
143	6.5	80.5	3.17	115	46.5	142.5	1.28
139	24.5	74.5	2.48	140	44.5	54.5	0.29
130	66.5	78.5	2.32	147	10.5	76.5	0.96
128	56.5	84.5	1.99	123	66.5	80.5	1.12
125	60.5	62.5	1.91	157	8.5	126.5	1.17
144	46.5	124.5	1.87	117	52.5	118.5	0.68
154	18.5	104.5	1.75	118	56.5	86.5	0.87

Table 5. The locations and ecoregion indices for the observation sites in the NSS, NECOSS1, and NECOSS2 experiments.

NSS			NECOSS1			NECOSS2		
Ecoregion Index	Lat	Lon	Ecoregion Index	Lat	Lon	Ecoregion Index)	Lat	Lon
115	58.5	62.5	115	58.5	62.5	115	58.5	62.5
115	46.5	142.5	115	46.5	142.5	137	26.5	92.5
137	26.5	92.5	137	26.5	92.5	157	8.5	126.5
115	54.5	84.5	137	28.5	118.5	123	66.5	80.5
115	52.5	120.5	157	8.5	126.5	147	10.5	76.5
137	28.5	118.5	123	66.5	80.5	117	48.5	132.5
137	26.5	104.5	147	10.5	76.5	121	60.5	148.5
137	46.5	54.5	121	60.5	148.5	166	0.5	110.5
115	62.5	132.5	166	0.5	110.5	118	56.5	86.5
137	34.5	72.5	117	52.5	118.5	155	-7.5	146.5

Table 6. The averaged statistics of surface CO_2 fluxes (gC m^{-2} yr^{-1}) for the experiments conducted in this study.

Exp. name	CNTL	CNTL_MOD	REDIST	ADD	SS	ECOSS	NSS	NECOSS1	NECOSS2	ALL
PC	0.965	0.966	0.973	0.977	0.98	0.984	0.983	0.987	0.986	0.998
BIAS	1.169	1.245	1.055	1.679	1.627	-0.211	-0.168	0.232	-0.28	-0.17
RMSD	70.06	70.528	60.547	54.708	53.572	45.388	47.034	41.9	42.218	15.947
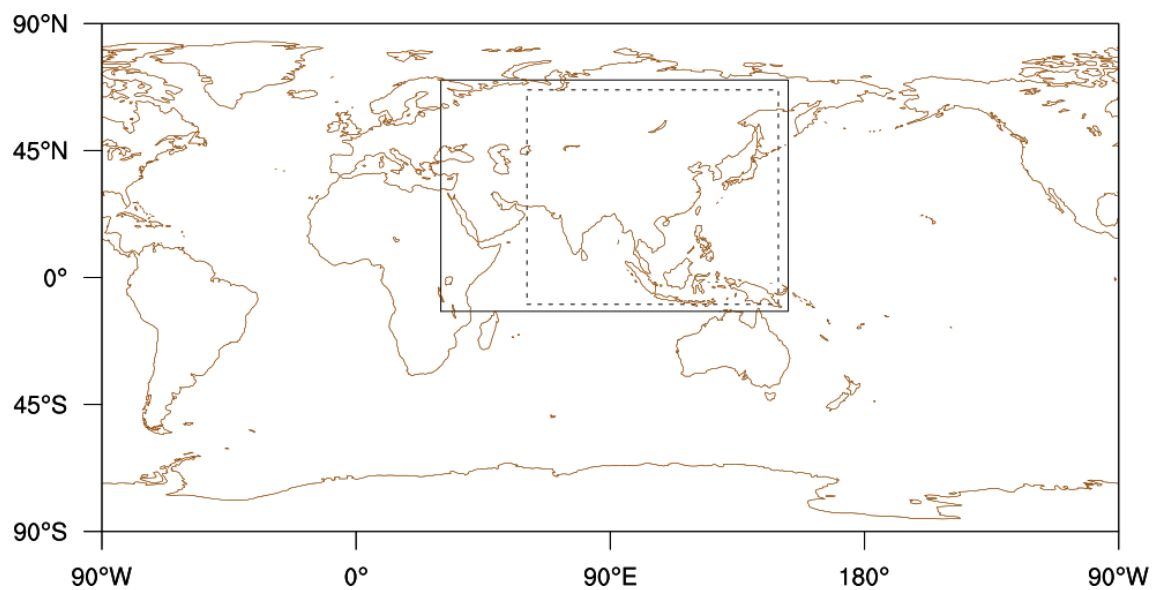
Figure 1. The distribution of the nested TM5 model domain over Asia (black solid rectangle) and verification domain (black dashed rectangle) used in this study.

Atmospheric
Chemistry
and Physics
Discussions

Open Access
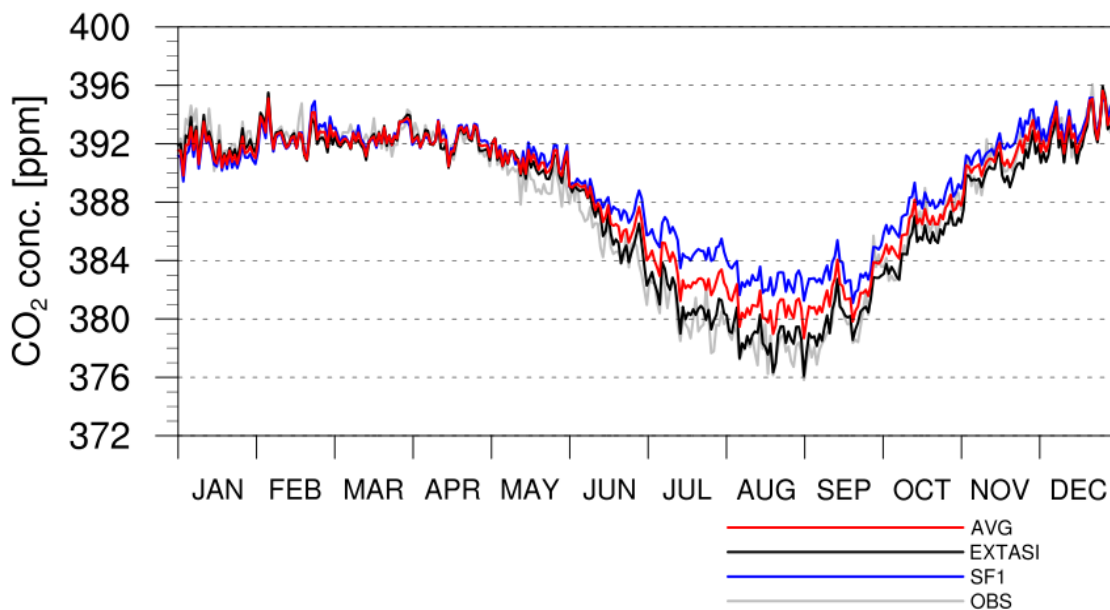
Figure 2. Time series of CO_2 concentration from hypothetical observations, model simulations, and real observations. The gray solid line (OBS) denotes the value of real observation data, the black solid line indicates the value from the EXTASI experiment, the blue solid line denotes the value of the SF1 experiment, and the red solid line denotes the average of the EXTASI and SF1, which regarded as True observation data in this study.
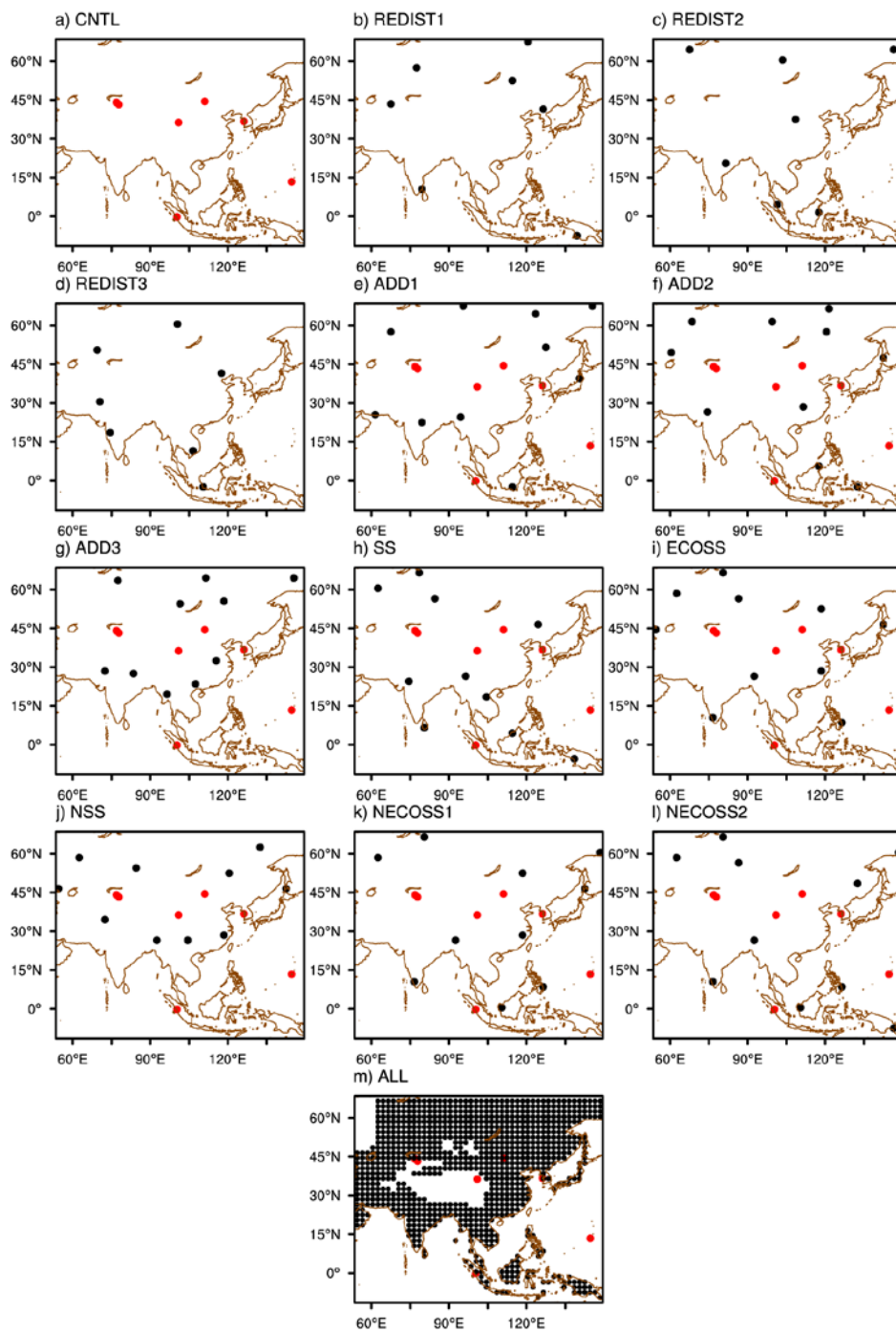
Figure 3. The distribution of observation sites in each observation network: a) the CNTL and
CNTL_MOD, b–d) the REDIST, e–g) the ADD, h) the SS, i) the ECOSS, j) the NSS, k) the NECOSS1,
l) the NECOSS2, and m) the ALL experiment. Red dots denote the observation sites of the NOAA
observation network and black dots denote the hypothetical observation sites.

41
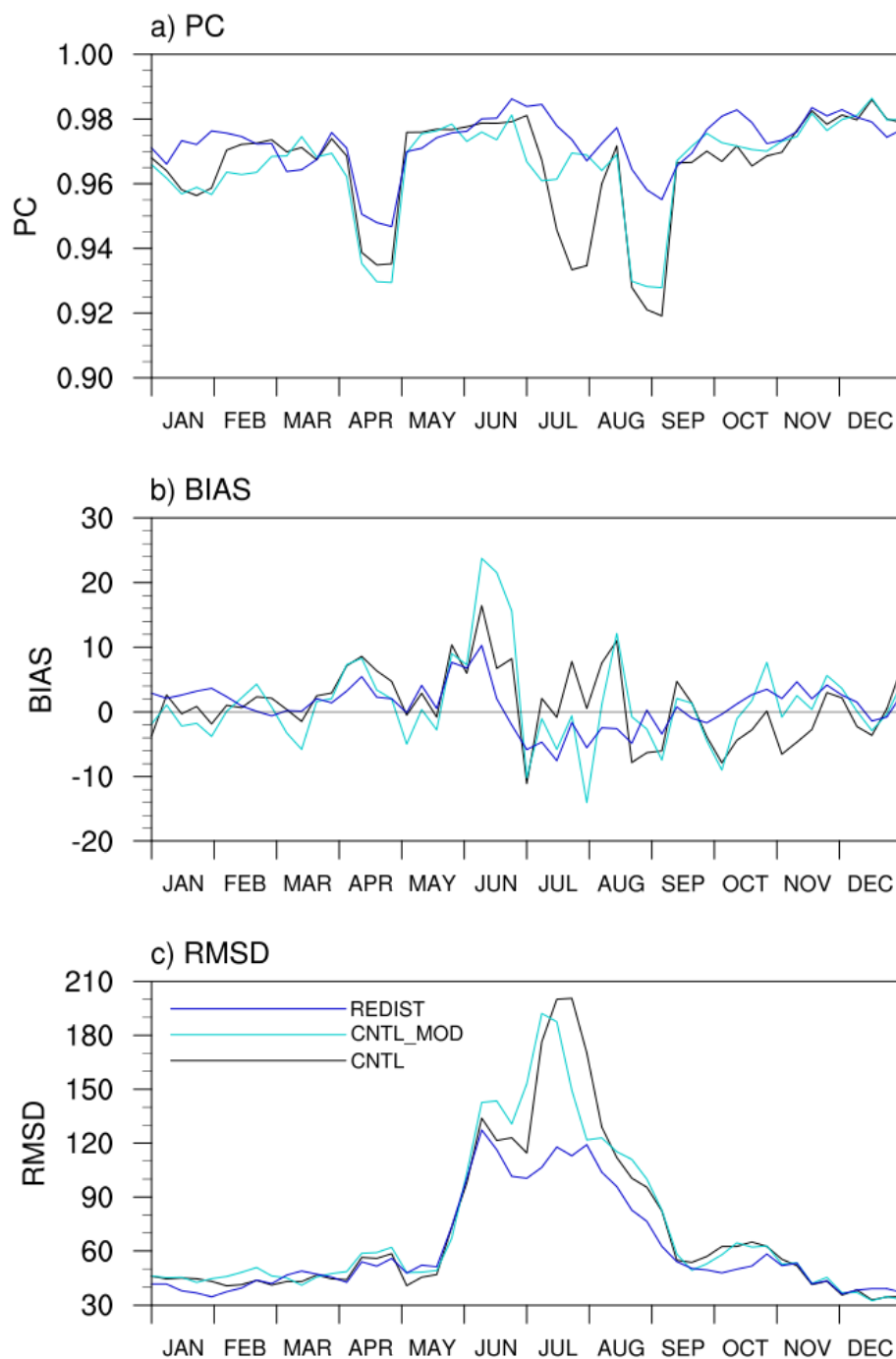
Figure 4. Time series of the three-week moving average of a) PC, b) BIAS, and c) RMSD of surface CO_2 flux (gC m^{-2} yr^{-1}) for the CNTL (black solid line), CNTL_MOD (cyan solid line), and REDIST (blue solid line) experiments.

Atmospheric
Chemistry
and Physics
Discussions
Open Access
EGU
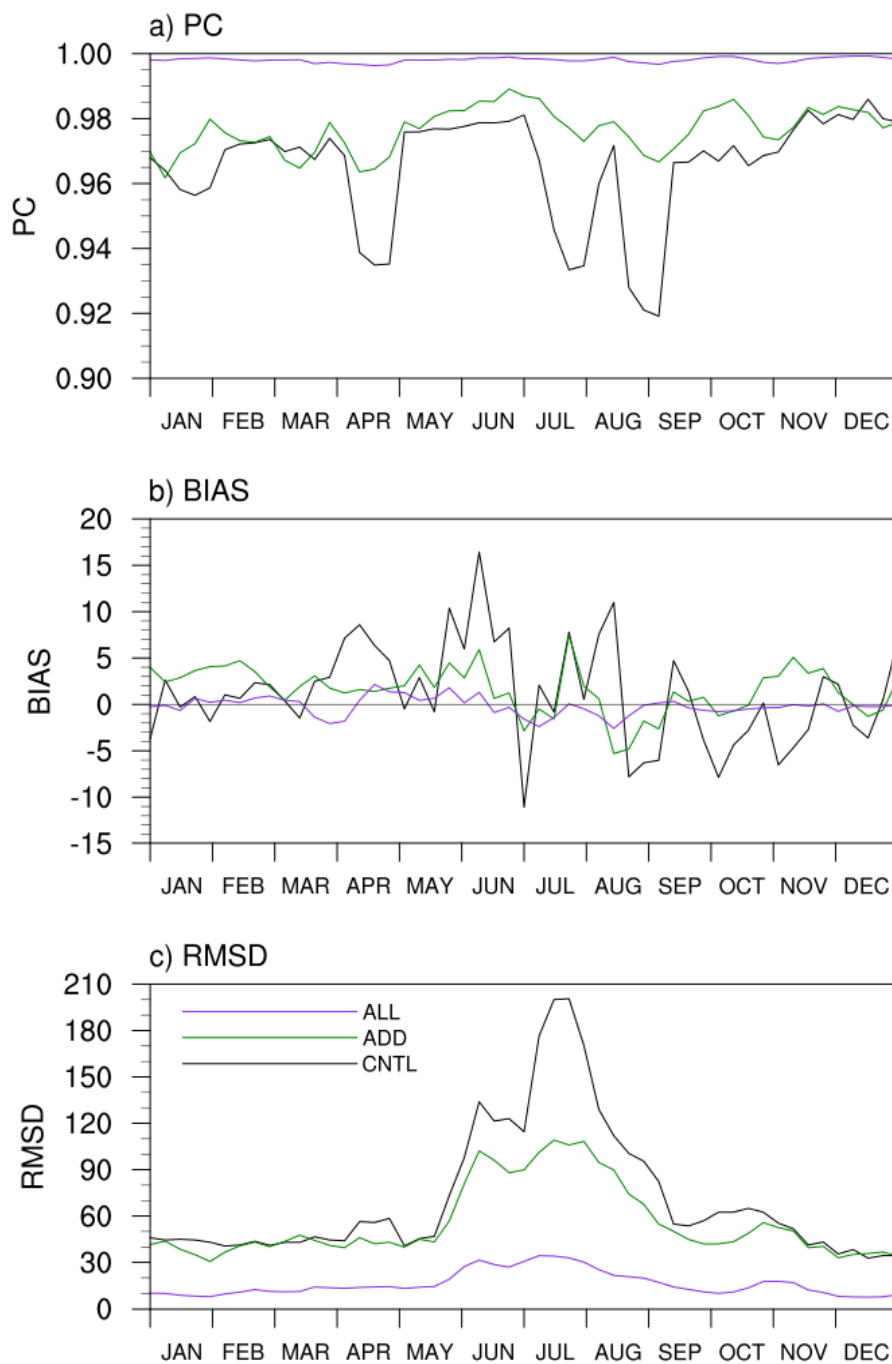
Figure 5. The same as Fig. 4 except for the CNTL (black solid line), ADD (dark green solid line), and ALL (purple solid line) experiments.
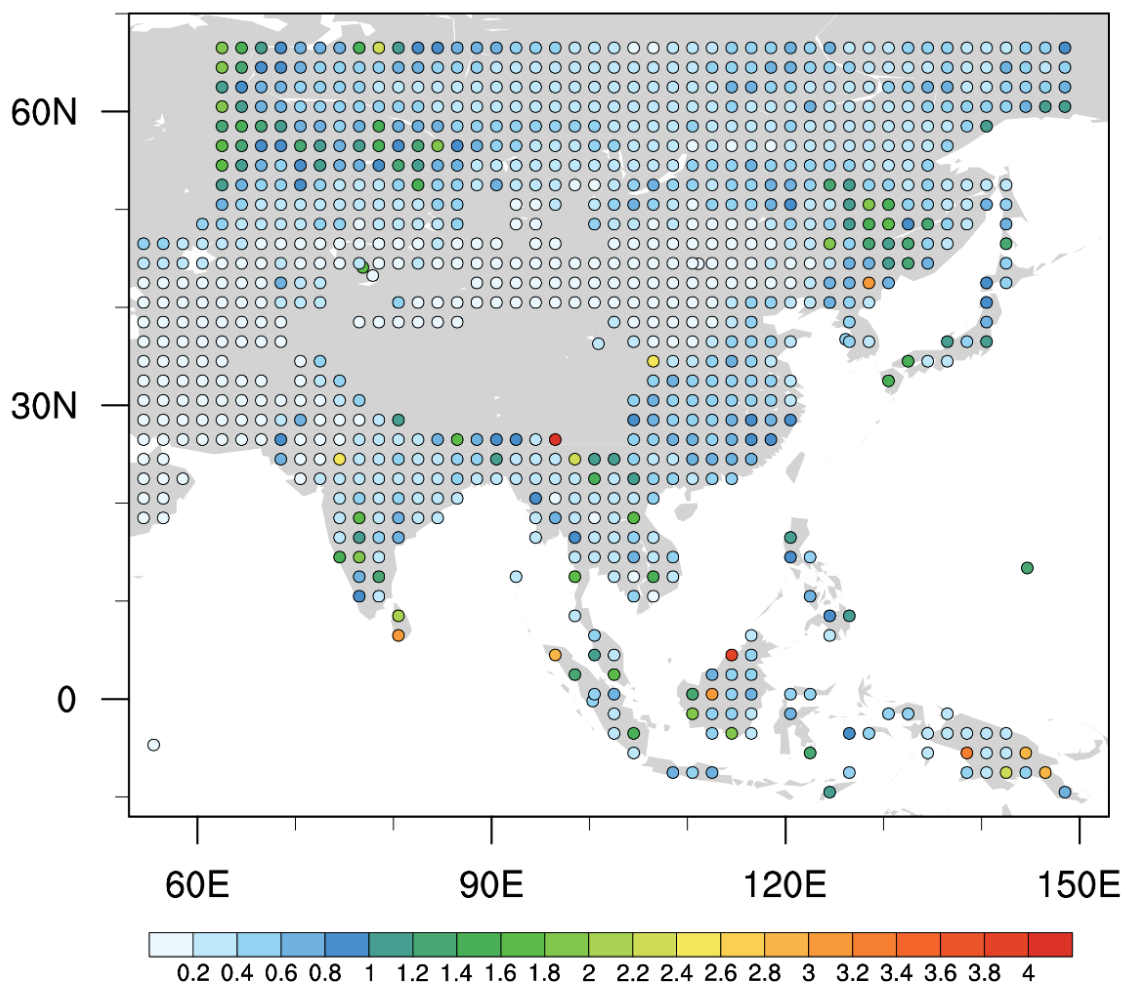
Figure 6. The spatial distribution of self-sensitivities (%) during the experimental period obtained from the ALL experiment.
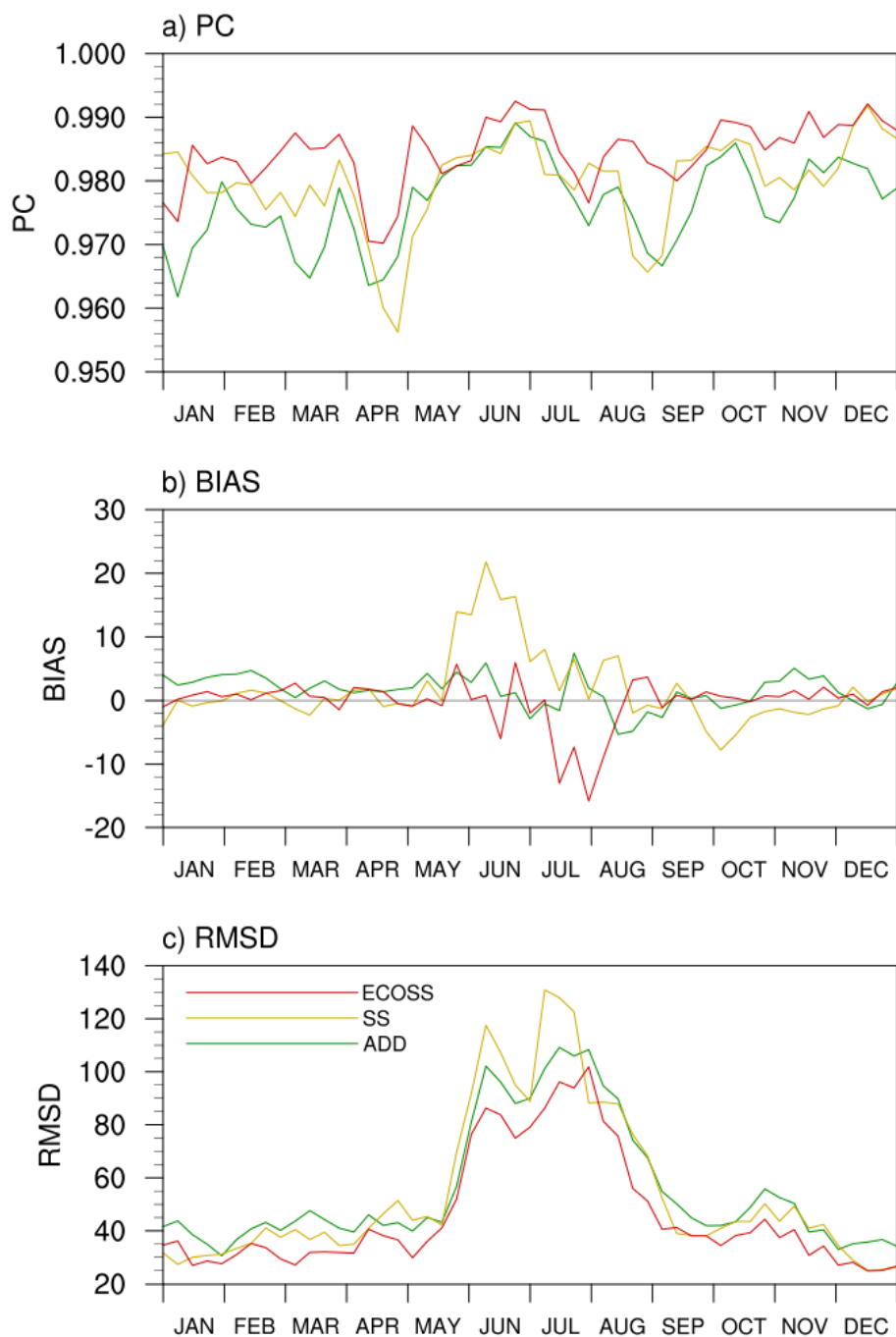
Figure 7. The same as Fig. 4 except for the ADD (dark green solid line), SS (yellow solid line), and ECOSS (red solid line) experiments.
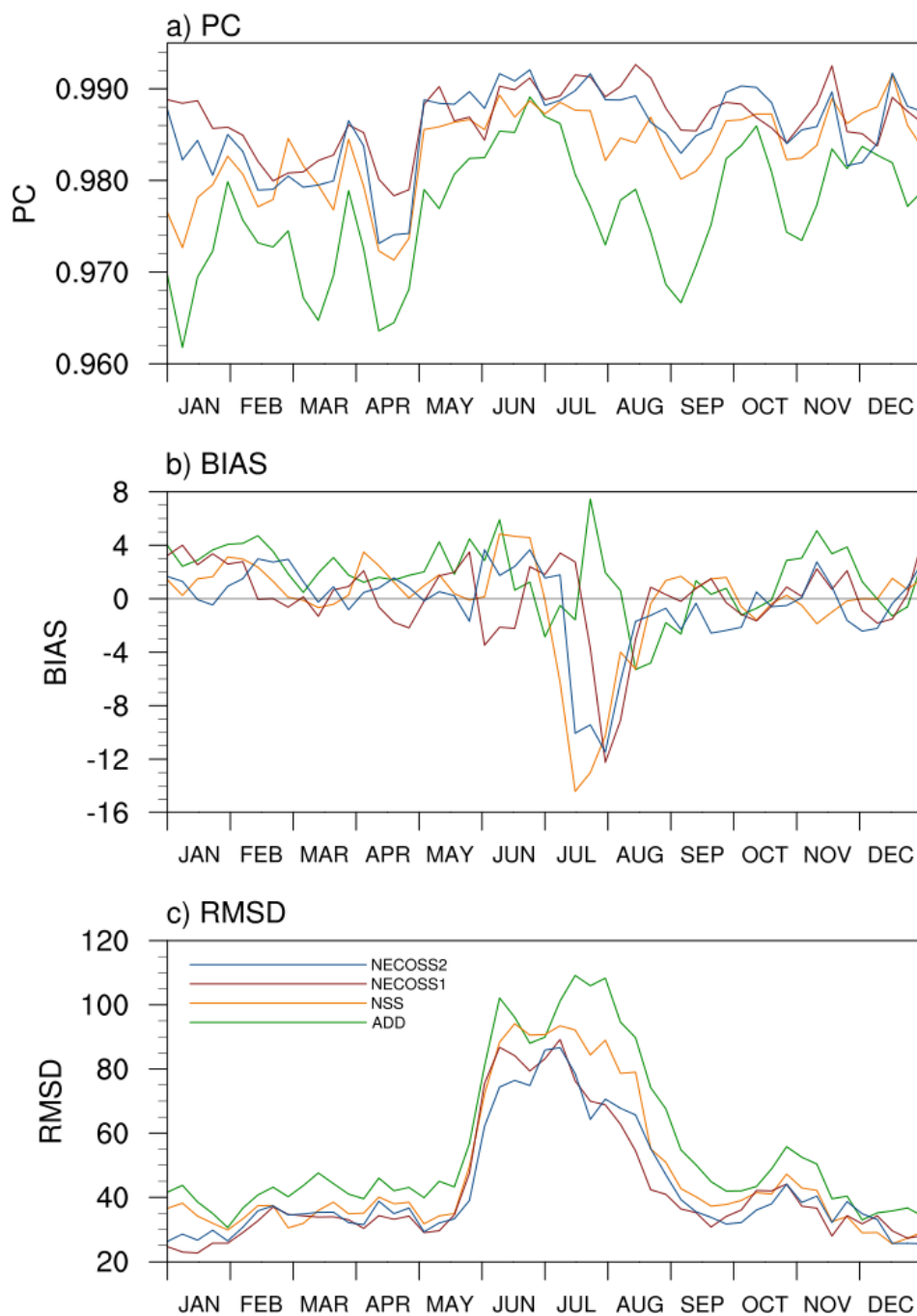
Figure 8. The same as Fig. 4 except for the ADD (dark green solid line), NSS (dark orange solid line), NECOSS1 (dark red solid line), and NECOSS2 (navy blue solid line) experiments.
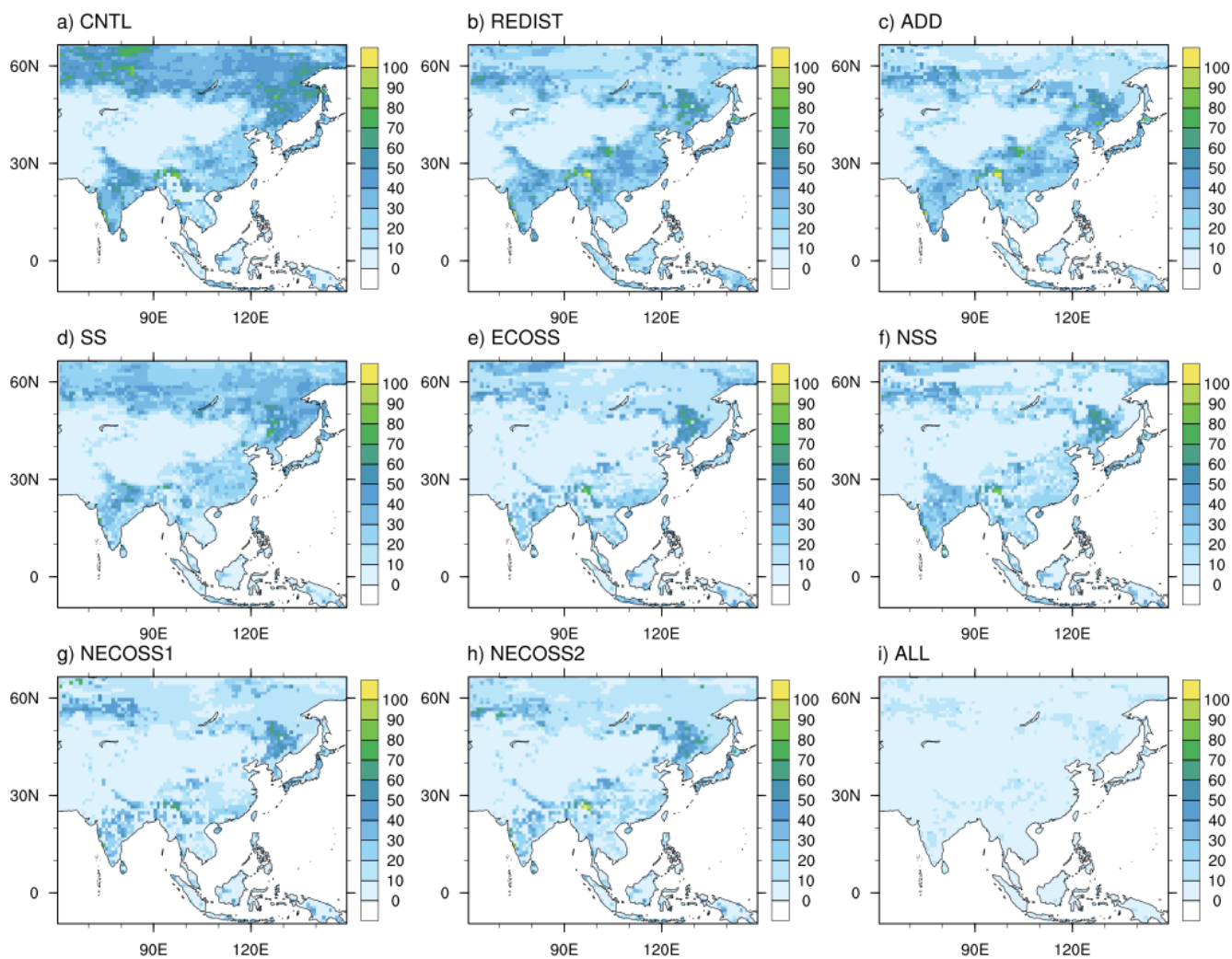
Figure 9. The spatial distribution of the average of weekly RMSD of surface CO_2 fluxes (gC m^{-2} yr^{-1}) for a) the CNTL, b) the REDIST, c) the ADD, d) the SS, e) the ECOSS, f) the NSS, g) the NECOSS1, h) the NECOSS2, and i) the ALL experiments.
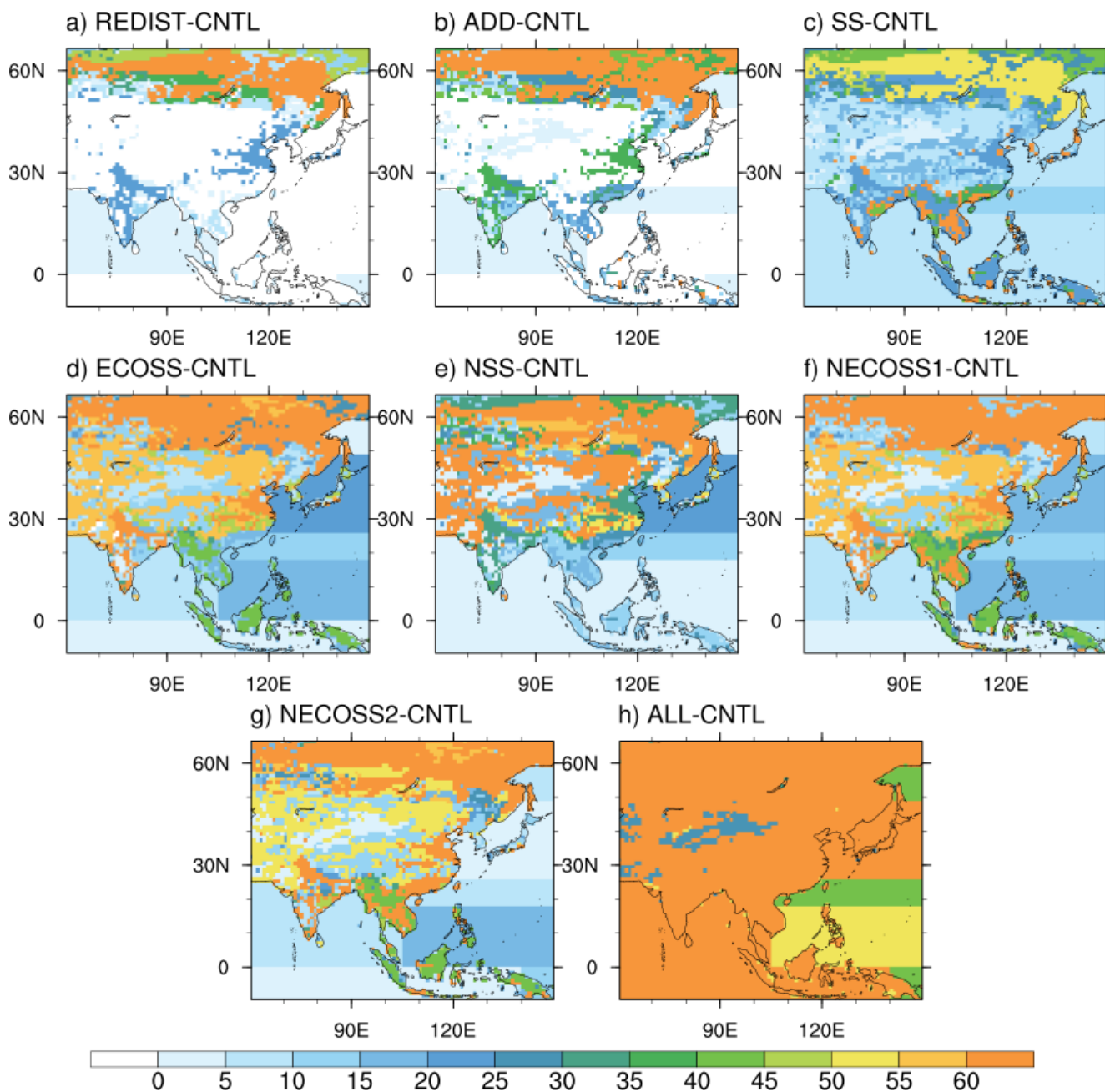
5

Figure 10. The spatial distribution of uncertainty reduction (%) for a) the REDIST, b) the ADD, c) the SS, d) the ECOSS, e) the NSS, f) the NECOSS1, g) the NECOSS2, and h) the ALL experiment, against the CNTL experiment.

5